scientific reports

Check for updates

OPEN

ATP synthase interactome analysis identifies a new subunit *l* as a modulator of permeability transition pore in yeast

Chiranjit Panja✉, Aneta Wiesyk, Katarzyna Niedźwiecka, Emilia Baranowska & Roza Kucharczyk✉

The mitochondrial ATP synthase, an enzyme that synthesizes ATP and is involved in the formation of the mitochondrial mega-channel and permeability transition, is a multi-subunit complex. In *S. cerevisiae*, the uncharacterized protein Mco10 was previously found to be associated with ATP synthase and referred as a new 'subunit *l*'. However, recent cryo-EM structures could not ascertain Mco10 with the enzyme making questionable its role as a structural subunit. The N-terminal part of Mco10 is very similar to *k*/Atp19 subunit, which along with subunits *g*/Atp20 and *e*/Atp21 plays a major role in stabilization of the ATP synthase dimers. In our effort to confidently define the small protein interactome of ATP synthase we found Mco10. We herein investigate the impact of Mco10 on ATP synthase functioning. Biochemical analysis reveal in spite of similarity in sequence and evolutionary lineage, that Mco10 and Atp19 differ significantly in function. The Mco10 is an auxiliary ATP synthase subunit that only functions in permeability transition.

Mitochondria, the dynamic organelles of endosymbiotic origin, are the source of cellular energy in the form of ATP necessary for life and at the same time they are the origin of intrinsic signals directing the cell into programmed death pathway[1,2]. Apart from ATP synthesis by the ATP synthase complex in the process of oxidative phosphorylation, OXPHOS[3], mitochondria is the hub for synthesis of metabolites, Fe-S clusters and essential amino acids[4]. The *Saccharomyces cerevisiae* as a model have provided fundamental insights into mitochondrial biology thanks to its ability to survive under fermenting conditions when OXPHOS is inactivated due to mutations in the structural and regulatory proteins of this system[5].

The ATP synthase monomer complex of *S. cerevisiae* and mammals is composed of 17 known subunits. It is organized into a membrane-embedded F_O domain and membrane-extrinsic F_1 catalytic domain connected by two stalks: central and peripheral. The F_O domain is built from the ring of ten subunits *c*/Atp9, subunit *a*/Atp6 and the small subunits Atp8, *i*/Atp18, *f*/Atp17, and membrane part of subunit *b*/Atp4. The matrix part of subunit *b*, together with subunits *h*/Atp14, *d*/Atp7, *OSCP*/Atp5, forms the external stalk connecting the F_O with the top of the F_1. The hydrophilic F_1 domain built from the hexamer of subunits $\alpha_3\beta_3$ and the central stalk built from subunits γ/Atp3, δ/Atp16 and ε/Atp15, are connected to the *c*-ring by subunit γ[6]. The ATP synthase monomers form dimer connected by subunits *a*/Atp6 interaction[7] and stabilized by the supernumerary subunits (subunits that are not essential for the catalytic activity) *e*/Atp21, *g*/Atp20 and *k*/Atp19[8–10]. Very little is known about the role of subunit *k*/Atp19. It is the homolog of mammalian subunit *k*/DAPIT, knock-out of which reduces ATP synthesis and destabilize the dimers[9]. Similarly, lack of *k*/Atp19 reduces dimers formation in *S. cerevisiae*[11]. Mutation in the gene encoding subunit *k*/DAPIT has been reported to result in Leigh syndrome in humans due to the reduced dimer formation and impaired ATP synthesis[12].

In the last decade, several groups demonstrated the involvement of ATP synthase in mitochondrial mega-channel formation (also called the permeability transition pore, PTP). However, despite extensive research in the field, the exact composition and molecular mechanism of the PTP still remain a mystery to be solved[13,14]. The PTP is defined as a Ca^{2+}-activated channel of the inner mitochondrial membrane which mediates the permeability to solutes up to 1.5 kDa[15,16]. It was demonstrated that the PTP resides in the *c*-ring and is gated by the F_1 dissociation[17,18]. The ATP synthase dimer junction may also be involved[19,20]. The ATP synthase subunits were shown to be a targets of the mega-channel inducers: the Ca^{2+} ions bind to β subunit while OSCP is involved in

Institute of Biochemistry and Biophysics, Polish Academy of Sciences, Warsaw, Poland. ✉email: chiranjit@ibb.waw.pl; roza@ibb.waw.pl

reactive oxygen species modulation of PTP. The adenine nucleotide transporter (ANT) was also found to contribute to the pore opening[21–25]. The primary consequence of PTP activation, when it opens for a long time, is the inner mitochondrial membrane depolarization followed by matrix swelling and rupture of the outer membrane. This process releases the pro-apoptotic factors and is being increasingly appreciated to be at the center of cellular death cascade[26–30]. Search of a pharmacological targets to inhibit PTP as a cure in several neuro-muscular diseases is a very active area of research[31–33].

Most of the ATP synthase subunits are small proteins in the range 5–20 kDa. In addition to the structural subunits *c*, *8*, *d*, *h*, *i*, *f*, δ and ε, this group includes hydrophobic supernumerary subunits *e*, *g*, *k*. Also, most of the small regulatory proteins known to interact with ATP synthase are within this molecular weight range[34]. However, identification of these proteins by mass spectrometry and western blot remains difficult due to their very low abundance, poor fragmentation and hydrophobic nature[35]. In this work, we analyzed extensively proteins in this molecular weight range binding to ATP synthase of *S. cerevisiae* and human, that we defined as 'small protein interactome of ≤ 20 kDa'. In an effort to differentiate how this interactome varies when ATP synthase undergoes dimerization, we further analyzed the proteins that remains associated with the monomers and the dimers. This work focuses on the characterization of the function of one protein Mco10 (Mitochondrial class one protein of 10 kDa) encoded by the *YOR020W-A* gene in *S. cerevisiae*. Mco10 and its homolog in *P. angusta* were also previously identified with ATP synthase in a pull-down experiment and was named as a new subunit *l*[36,37]. The N-terminal part of this protein is very similar in sequence to subunit *k*/Atp19, homologs of which were also present in those species. Interestingly, Mco10 and its homolog in *P. angusta* were not present in subsequent cryo-EM structures, thus demonstration that Mco10 is a bona fide subunit of ATP synthase complex is missing[6,38,39]. In this work, we present evidence that Mco10 is indeed an ATP synthase subunit in *S. cerevisiae*. Phylogenetic analysis of Mco10 and Atp19 in fungal species further showed that many related yeast species maintain the two proteins and Mco10 is evolutionarily more ancient. However, Mco10 and Atp19 functions are significantly different. Mco10 has a role in modulating the mitochondrial mega-channel and calcium homeostasis, unlike Atp19, which does not modulate PTP. Our results indicate that small unknown proteins can play important role in cell physiology[40].

Material and methods

Yeast strains and growth media. Strains of *Saccharomyces cerevisiae* used in the study were BY4741 (*MATa his3Δ1; leu2Δ0; met15Δ0; ura3Δ0*) and isogenic *Δatp19*, *Δatp20*, *Δatp21* and *Δmco10* (Euroscarf collection). The double mutant *Δatp19 Δmco10* was constructed by crossing the single mutants in the opposite mating sign and tetrad dissection. MR6 (*MATa ade2-1 his3-1,15 leu2-3,112 trp1-1 ura3-1 arg8::HIS3*) expressing Atp6-HA-6His was a gift from prof. Alexander Tzagoloff (Columbia University, NY, USA). Strains were grown in rich YPGA medium (1% Bacto yeast extract, 1% Bacto peptone, 2% glucose, 40 mg/L adenine), YPGlyA medium (1% Bacto yeast extract, 1% Bacto peptone, 2% glycerol, 40 mg/L adenine) or W_0 complete minimal medium (6.7% yeast nitrogen base w/o amino acids and 2% glucose, supplemented with appropriate drop-out amino acid stock (Sunrise)) at 28 °C or 36 °C with shaking at 200 rpm. The liquid media were solidified by addition of 2% Bacto agar (Difco, Becton Dickinson). For mitochondria isolation, strains were grown in rich YPGlyA medium to an OD_{600} of 4. An OD_{600} of 1 corresponds to 1.2×10^7 cells/mL. G418 sulphate were added to media at a concentration of 200 µg/mL.

Purification of ATP synthase complexes from mitochondria. The strain expressing Atp6 subunit C-terminally tagged by HA-6xHis in the mitochondrial genome was characterized previously to cause no damage to the ATP synthase structure[41]. This strain was used to pull down the whole ATP synthase complex by Ni-NTA agarose beads. Briefly, 5 mg of mitochondria were centrifuged and suspended in 1 mL of sonication buffer (250 mM sucrose, 50 mM NaH_2PO_4, 5 mM 6-aminocaproic acid, 1 mM EDTA, pH 7.5, protease inhibitors cocktail tablet (Roche), 1 µM PMSF) and sonicated 6 times 10 s, with 10 s intervals on ice. After centrifugation at 6000 × g 10 min at 4 °C, supernatant was ultracentrifuged at 268,526 × g for 1 h (Thermo Scientific™ Sorvall™ WX ultracentrifuge, TFT80.2 rotor). The pellet was washed twice with the sonication buffer without EDTA (without suspending it) and then suspended with the use of the potter in 500 µl MP extraction buffer (150 mM potassium acetate, 10% glycerol, 2 mM 6-aminocaproic acid, 30 mM HEPES, pH 7.4, 1% N-dodecyl-β-maltoside, 2 mM PMSF and protease inhibitors cocktail tablet, EDTA-free, Roche). After 20 min incubation on ice, the membranes were centrifuged for 30 min at 21,950 × g, 4 °C and the extract was incubated with 200 µL of the Ni–NTA agarose washed previously by Binding buffer (50 mM NaCl, 10% glycerol, 10 mM imidazole, 20 mM NaH_2PO_4, pH = 7.9, 0,1% n-dodecyl-β-maltoside, 2 mM PMSF, protease inhibitors cocktail tablet) for overnight. Next day the beads were washed twice with the Binding buffer, then suspended in 400 µL of Binding buffer, dosed and after addition of 100 µL of 5 × Laemmli sample buffer, boiled during 5 min. The 50 µg of the extract and 2 µg of bead eluate were loaded on the 15% SDS-PAGE gel. Then the gel was stained with Coomassie blue or silver staining according to manufacturer's protocol (Pierce sliver stain kit, Thermo Fisher Scientific) to visualize the proteins.

Isolation of mitochondria from HEK293T cells. HEK293T (ATCC) cells were maintained in media composed of DMEM (high glucose; Biowest), sodium pyruvate (Thermo Fisher Scientific), stable glutamine (Biowest), non-essential amino acids (Thermo Fisher Scientific), 10% fetal bovine serum (EurX), and penicillin/streptomycin solution (Thermo Fisher Scientific). Cells were cultured to confluence on six 9 cm plates. Mitochondria were isolated by differential fractionation previously described[42] with minor adjustments. Briefly, cells were washed 2 × with ice-cold PBS. The PBS buffer was removed and the cells were scraped in ice-cold NKM buffer (1 mM Tris–HCl pH 7.4, 130 mM NaCl, 5 mM KCl, 7.5 mM MgCl) and incubated on ice for 5 min. Then 100 µl of 10xHomB buffer (225 mM mannitol, 75 mM sucrose, 10 mM HEPES–NaOH pH 7.8, 10 mM

EDTA) per 1 mL of homogenate with protease and phosphatase inhibitors was added and homogenized using a Dounce homogenizer with nuclei release and integrity monitored microscopically. The nuclear fraction was separated using two rounds of centrifugation at 900 × g for 5 min at 4 °C. The supernatant was then centrifuged at 10,000 × g for 10 min to isolate crude mitochondrial pellet. The pellet was suspended in Blue Native protein extraction buffer, dosed and ATP synthase complex from 400 µg μ of protein was extracted with 2% Digitonin. The dimers and monomers were separated in 3–12% gradient gel followed by SDS-PAGE separation in second dimension and bands from 5–20 kDa region from Coomassie stained gel from the monomers and dimers were subjected to mass spectrometric analysis.

Production of Mco10 antibody. The Mco10 specific antibody was generated using a peptide KDDDVVKSIEGFLNDLEKDTRQDT identical to the Mco10 fragment from 64 to 83 amino acids residues. The immunization of rabbit, isolation and the affinity purification of polyclonal antibodies was performed by Davids Biotechnologie GmbH (Germany).

Two Dimensional BN-PAGE/SDS-PAGE and Western blotting. Two-dimensional gel electrophoresis was based on the protocol of Schamel[43] with slight modifications. Briefly, the ATP synthase complexes were liberated from inner mitochondrial membrane of isolated mitochondria by incubation with 1–2% digitonin in extraction buffer (30 mM HEPES, 150 mM potassium acetate, 12% glycerol, 2 mM 6-aminocaproic acid, 1 mM EGTA, protease inhibitor cocktail tablets EDTA-free (Roche), pH 7.4) for different time intervals up to 60 min and separated using NativePAGE™ 3–12% Bis–Tris Gels (Thermo Fisher Scientific) to separate monomeric and dimeric ATP synthase complexes[44]. For second dimensional analysis the lanes were cut from the gel and placed in SDS-PAGE running buffer (25 mM Tris, 192 mM Glycine, 0.1% SDS, pH 8.3 with 1% β-mercaptoethanol), heated in a microwave for 10 secs and incubated for another 10 min in a shaker. The gel strips were then loaded on the top of a 16% SDS-PAGE gel, and electrophoresis was conducted under denaturing conditions. Then the gel was stained with Coomassie blue or silver staining and bands cut-off were analyzed by mass spectrometry. For Western blotting proteins from the gel were transferred into PVDF or nitrocellulose membranes using iBlot system (Thermo Fisher Scientific). For SDS-PAGE analysis of steady state level of proteins, yeast cells were disrupted by alkaline lysis with NaOH/TCA[45]. Western blot analysis was performed using the polyclonal rabbit anti-Mco10 antibody, anti-ATP synthase subunits antibodies (gifts from Marie-France Giraud, Bordeaux, France and Martin van der Laan, Germany), anti-Rip1 and Cob1 antibodies (provided by dr hab. Ulrike Topf, IBB PAS) or anti-Cox2 (Thermo Fisher Scientific).

Mass spectrometry analysis. The 5–20 kDa proteins containing fragments of SDS-PAGE gels were cut out, de-stained and subjected to in-gel tryptic digestion. The tryptic digested peptides were then independently analyzed by LC/MS system at the IBB PAS Mass Spectrometry Facility unit using Evosep One (Evosep Biosystems, Odense, Denmark) coupled to a Orbitrap Exploris 480 mass spectrometer (Thermo Fisher Scientific, Bremen, Germany) via Flex nanoESI ion source[46] or by Thermo EASY-nLC 1000 system interfaced to Thermo Fisher LTQ Orbitrap Elite and Velos. Peptides were then loaded on a trapping column and eluted over a C18 75 µm (Elite/Velos) or 150 µm (Exploris 480) analytical column at 250 nL/min. The mass spectrometer was operated in data-dependent mode. MS1 scan range of 300 to 1600 m/z was selected and top 40 precursors within an isolation window of 1.6 m/z were considered for LC/MS analysis. Data were acquired in positive mode with a data-dependent method using the following parameters: the raw data were then searched using an inhouse copy of Mascot with the following parameters: Enzyme: Trypsin, Database: SGD_new (6,713 sequences; 3,019,540 residues) or Sprot_02 (567,483 sequences; 204,940,973 residues) with Carbamidomethyl (C) as fixed modification and Oxidation (M), Acetyl (N-term, K), Phospho (S, T, Y), GlyGly (K) as variable modifications, Mass values: Monoisotopic, Peptide Mass Tolerance: ± 5–10 ppm, Fragment Mass Tolerance: ± 0.01–0.1 Da, Max Missed Cleavages: 2 and rejected all proteins found in cRAPome database during analysis.

Measurement of oxygen consumption, ATP synthesis and membrane potential. Mitochondria were isolated from cells grown in YPGlyA medium at 28 °C by enzymatic method according to the protocol described previously[47]. For all assays, they were diluted to 75 µg/mL in respiration buffer (10 mM Tris-maleate pH 6.8, 0.65 M mannitol, 0.35 mM EGTA, and 5 mM Tris–phosphate). Oxygen consumption rates were measured using a Clarke electrode adding consecutively 4 mM NADH (state 4 respiration), 150 µM ADP (state 3) or 4 µM carbonyl cyanide m-chlorophenylhydrazone (CCCP) (uncoupled respiration), as described previously[48]. The rates of ATP synthesis were determined under the state 3 conditions with 750 µM ADP; every 15 s, 100 µl aliquots were withdrawn from the oxygraph cuvette and added to 50 µl of the 3.5% (w/v) perchloric acid and 12.5 mM EDTA solution already prepared in the tubes to stop the reaction. The samples were then neutralized to pH 6.5 by the addition of KOH and 0.3 M MOPS. The synthetized ATP was quantified using a luciferin/luciferase assay (Kinase-Glo Max Luminescence Kinase Assay, Promega) in a Beckman Coulter Paradigm plate reader. The participation of F_1F_O-ATP synthase in ATP production was assessed by measuring the sensitivity of ATP synthesis to oligomycin (3 µg/mL). The specific ATPase activity at pH 8.4 of non-osmotically protected mitochondria was measured using the procedure previously described[49]. The oxygen consumption was quantified in nmol O_2 min^{-1} mg^{-1}, the ATP synthesis in nmol of ATP min^{-1} mg^{-1} and ATPase activities in µmol Pi min^{-1} mg^{-1}. Variations in transmembrane potential ($\Delta\Psi$) were evaluated by monitoring the fluorescence quenching of Rhodamine 123 (0.5 µg/mL; λ_{exc} of 485 nm and λ_{em} of 533 nm) from mitochondrial samples (0.150 mg/mL) in the respiration buffer under constant stirring at 28 °C using a Cary Eclipse Fluorescence Spectrophotometer (Agilent Technologies, Santa Clara, CA, USA) as described previously[50].

Measurement of the mitochondrial calcium retention capacity and swelling. A previously developed method for measurement of mitochondrial calcium retention capacity (described in detail in[19]) was used to measure the time of yPTP opening after Ca^{2+} addition. Briefly, isolated mitochondria were diluted in CRC buffer (250 mM sucrose, 10 mM Tris-MOPS, 10 µM EGTA-Tris, 5 mM P_i-Tris, 1 µM Calcium Green-5N (Thermo Fisher), 0.5 mg/mL BSA, pH 7.4) to a concentration of 1 mg/mL. The reaction was started by adding 1 mM NADH and 5 µM of Calcium ionophore ETH129. After equilibration for 1 min, 200 µM $CaCl_2$ was added. The rapid increase in the fluorescence of Calcium Green-5N after sometime was attributed to the release of calcium ions from the mitochondrial matrix into the buffer, likely due to the opening of the permeability transition pore. Matrix swelling was evaluated by measuring optical density changes at 540 nm with a Parkin Elmer Lambda 925 UV–Vis spectrophotometer. Mitochondria (500 µg/mL) were suspended in 2 mL of swelling buffer (150 mM sucrose, 10 mM Tris–HCl, 2 mM KH_2PO_4, pH 7.4) and then, 2 mM $CaCl_2$ and 10 µM alamethicin were added[51].

Phylogenetic tree construction. The first 25 amino acids of Mco10 or Atp19 of *S. cerevisiae* were used as templates to identify homologs of these proteins from the published fungal genomes using BlastP. The phylogenetic tree was constructed using homologous sequences from model *Ascomycota* and *Basidiomycota*. Maximum Likelihood phylogenetic inference was performed in MEGA X software[52] with a Poisson correction model[53]. Initial tree(s) for the heuristic search were obtained automatically by applying Neighbor-Join and BioNJ algorithms to a matrix of pairwise distances estimated using the Poisson model, and then selecting the topology with superior log likelihood value.

Structural analysis. Multiple sequence alignment of Atp19 and Mco10 was performed using ClustalOmega[54]. Hydropathy plots were generated by ProtScale on the ExPASy Server using Kate and Doolittle for predicted proteins of *S. cerevisiae*. Homology modelling of the ATP synthase complex was based on the atomic model built in the cryo-electron microscopy density map of *S. cerevisiae* ATP synthase, PDB: 6B8H[6], and Alphafold2 predicted structures of subunits in *S. cerevisiae*[55,56]. Structures of the homologs of Mco10 and Atp19 in *Candida albicans* and *Pichia angusta* were analyzed using the available structures in Alphafold2 database and also verified using ColabFold which offers an accelerated protein structure predictions by combining MMseqs2 with AlphaFold2 or RoseTTAFold[57]. Structural visualization was carried out using PyMOL software.

Data and statistical analyses. To determine a high confidence small protein ATP synthase interactome, we emphasized more on manual validation due to poor performance of conventional algorithms which often rejects peptide fragments identified from these small proteins as false positive due to low score. Often, these are identified with a true single peptide hit but rejecting them makes the data underrepresented. To overcome this, we enriched the data using the following rules: all proteins identified with molecular weight ≥ 20 kDa were excluded from the analysis; proteins identified with single peptides were retained if identified in more than two independent analyses with protein coverage ≥ 10%. Most single peptide and low coverage identified proteins were further manually inspected to minimize false discoveries. Protein interaction network was constructed using STRING database with medium confidence level[58] and visualized using the STRING 106 plugin in Cytoscape. The identified proteins were classified manually or by Gene Ontology terms. Unless otherwise stated in the figure legends, each experiment was repeated at least three times. Data are presented as a representative experiment or as the average ± SD. To assess significant differences with the control and test samples, Student's t-test was used. For images acquisition the Uvitec Cambridge Q4 Alliance and the manufacturer`s software was used. All figures in this study were assembled using Microsoft Office PowerPoint or Adobe Photoshop (Adobe Inc.).

Results

Small protein interactome of ATP synthase. The full ATP synthase complex was pulled down by HA-6xHis-tagged Atp6 bound to Ni–NTA agarose. The proteins were then eluted from the beads, separated in the 15% SDS PAGE gel and visualized by silver staining. In another approach, the monomers and dimers of ATP synthase were extracted from isolated mitochondria by 2% digitonin, separated in 3–12% BN-PAGE, and then the monomers and dimers were resolved in a 2nd dimension 16% SDS PAGE (Fig. 1a). To compare the yeast interactome with human, the monomers and dimers of ATP synthase from mitochondria isolated from HEK293T were extracted with similar digitonin concentration as from yeast and similarly resolved in 2D-BN-SDS-PAGE. Gel lane fragments in the 5–20 kDa range were submitted for mass spectrometry identification as defined in the methods section (Supplementary Fig. S1, Supplementary Tables S1, S2 and S4).

From the analysis of *S. cerevisiae* samples, a total of 89 proteins from pull down experiment and 144 proteins from 2D-BN-SDS-PAGE got enriched according to the set criteria outlined in the methods. Among them, 75 proteins were commonly identified in both the experiments (Fig. 1b). All the eleven subunits of ATP synthase with mol. wt ≤ 20 kDa also got identified including the ATPase activity inhibitor protein Inh1. However, Atp8 were only identified in pull down and not detected from 2D-BN-PAGE samples. The result also showed that the three known supernumerary subunits *k*/Atp19, *g*/Atp20 and *e*/Atp21 were present in both the monomer and the dimer. The yeast interactome was also highly enriched with several ribosomal proteins which were more abundant in 2D-BN-SDS-PAGE. Also, we found several subunits of Complex IV including Cyt c and four members of Complex III to remain associated with ATP synthase in both approaches showing they form sub-complexes with ATP synthase. In addition, members of the Sec61 translocation complex, the chaperonin Hsp10 and member of the MICOS component Mic10 were identified in both the monomers and the dimers. Mic10 was previously shown to interact with the dimeric F_1Fo-ATP synthase[59]. Three uncharacterized proteins Yor020W-A (Mco10),

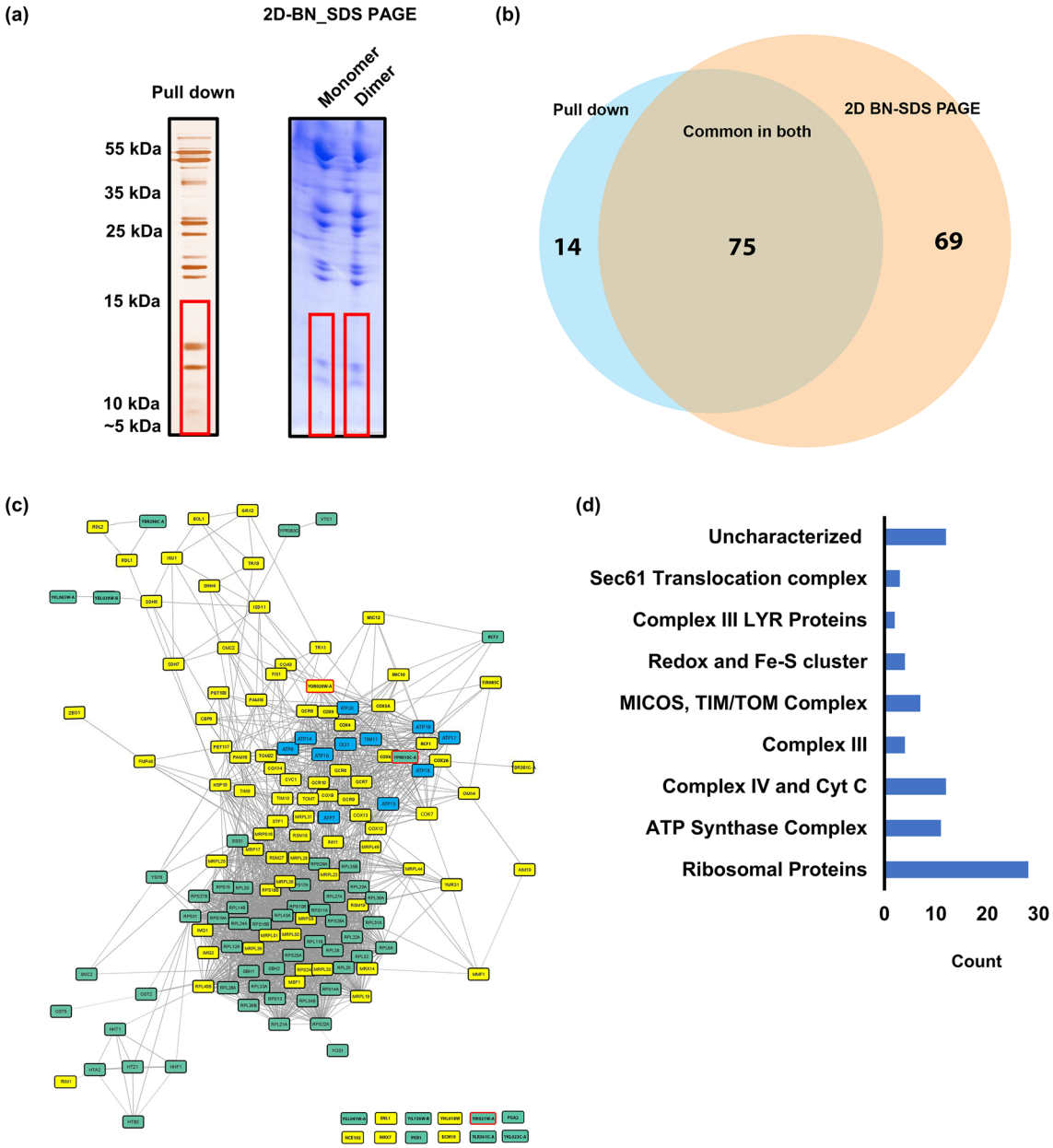

Figure 1. Small molecule interactome of *S. cerevisiae* ATP synthase. (**a**) Pulldown of ATP synthase complex by HA-6His-tagged Atp6 or the monomers and dimers of ATP synthase extracted by digitonin and separated in two-dimensional BN-SDS-PAGE gel and visualized by silver stain (left panel) or Coomassie (right panel). Gel pieces from region indicated by red frames were cut-off for LC/MS analysis. The experiments were performed many times and representative gels are shown. Original blots/gels are presented in SupplementaryRowImages pages 9 and 10. (**b**) Venn diagram of the ≤ 20 kDa proteins associated with ATP synthase identified in the interactome analysis from the two different approaches. (**c**) High confidence ATP synthase interactors identified by MS were connected into a network using the STRING database and visualized using the STRING 106 plugin in Cytoscape. Proteins marked in yellow are known proteins that localize to the mitochondria. Proteins marked in blue are the known ATP synthase subunits identified in the analysis. Proteins marked in green were not previously assigned to be localized to mitochondria. Mco10, Min8 and Yir021w-a are indicated by red frames. (**d**) Classification of the identified proteins into known complexes and processes.

Ypr010C-A (Min8), Yir021W-A, were enriched with ATP synthase in our study showing that they can potentially modulate ATP synthase in yet unknown way (Fig. 1c,d, Supplementary Table S1).

The human ATP synthase interactome of small proteins identified 136 proteins among which 16 proteins were only identified in the monomers and 21 proteins got identified only in the dimers (Fig. S2 and Supplementary Table S2). We identified all ten subunits of ATP synthase complex and the ATPase activity inhibitor protein within this defined mass. However, subunits *g*, *c* and the coupling factor 6 were identified only in the dimer sample. Several members of Complex IV and Complex I were also highly enriched. Homologs of many proteins outside

of the OXPHOS complexes, identified in yeast ATP synthase interactome, were also present in the human ATP synthase interactome, validating the yeast data. Examples include members of the SEC61 translocation complex or chaperonin HSP10.

Yor020W-A (Mco10) co-purifies with the ATP synthase complex. From the pull down and 2D-BN-SDS-PAGE analysis of the monomers and dimers of *S. cerevisiae* ATP synthase, the uncharacterized protein Yor020W-A (Mco10) was among the highly enriched and identified with more than 50 peptides and greater than 50% sequence coverage (Supplementary Fig. S3). However, it was only identified in the monomer in two replicates. As Mco10 was previously identified in a pull down of ATP synthase and hypothesized as its potential subunit[36] we set to characterize the Mco10 role in ATP synthase function.

Phylogenic analysis of Mco10 and Atp19 based on sequence similarity. Detailed comparison of the sequences of fungal homologs of Atp19 and Mco10 showed that these proteins have high similarity within their N-terminal part as noted previously[36]. *S. cerevisiae* Mco10 and Atp19 share around thirty percent sequence similarity, mainly within the N-terminal region (Fig. 2a). The serine rich hydrophilic middle region is characteristic for Mco10 and is absent in Atp19 (Fig. 2b). The structures of Mco10 and Atp19 were analyzed using the available structures in AlphaFold2 database (Fig. 2c). The structures of related proteins in *Candida albicans* and *Pichia angusta* were also analyzed using predicted models available in AlphaFold2 database (Supplementary Fig. S4). Mco10 and Atp19 (and the related homologs) mainly consists of two helices with a disordered middle region. The N-terminal helical region that is similar in sequence in both proteins align perfectly (by PyMOL software). Although the exact spatial positions of the C-terminal helices remain difficult to predict due to the poor accuracy of the middle region, but analysis of AlphaFold's expected position error PAE plot does give a fair confidence on their orientation in the predicted models (Fig. 2d). We performed an extensive phylogenetic analysis of the genes sequences of Atp19 and Mco10 and their related homologs that are present or are hypothesized to be present in the published genomes of fungi. We found that not only *S. cerevisiae* and *P. angusta*, but several closely related *Saccharomycetales* species have both paralogs. Phylogenetic inference showed a separate clade for Atp19/Mco10 homologs grouping solely *Saccharomycetales* sequences. Remaining taxa possess a single Atp19 protein suggesting the latter is the ancestral subunit. However, given the time scale these proteins have diverged, it is very likely that Atp19 and Mco10 gained independent additional features with respect to ATP synthase structure and function (Fig. 2e, Supplementary Fig. S5, Supplementary Table S3).

ATP synthase activity and mitochondrial membrane potential. To check if Mco10 is indeed attached to ATP synthase we first checked the respiratory growth of *Δmco10*, *Δatp19* and the double deletion *Δatp19Δmco10* mutants at 28 and 36 °C, the conditions of moderate heat stress for yeast where growth phenotypes, not only on respiratory medium are often more pronounced. As shown on Fig. 3a, the respiratory growth of these mutants is not affected. Then we supplemented the respiratory medium with suboptimal concentration of oligomycin, an ATP synthase inhibitor, which does not affect growth of the wild type strain. In these conditions deletion of Atp19 significantly reduces the growth at 1 µg/mL oligomycin at both growth temperatures. Deletion of Mco10 does not affect the respiratory growth under these conditions. Moreover, *Δmco10* was more resistant to oligomycin at 36 °C and its deletion in *Δatp19* background, i.e., in the double mutant, also partially rescued the growth at 28 °C (Fig. 3a).

We consequently asked whether lack of Mco10 affects the OXPHOS and ATP synthase activities in wild type and in *Δatp19* background. The oxygen consumption was measured in isolated mitochondria with NADH as an electron donor, alone (basal or state 4 respiration), and after successive addition of ADP (state 3, phosphorylating conditions) or CCCP (uncoupled, maximal respiration). At 28 °C, *Δmco10*, *Δatp19* or the double deletion *Δatp19Δmco10* mutants does not significantly affect oxygen consumption rates of mitochondria in all above conditions (Fig. 3b). We next measured the rate of ATP synthesis by ATP synthase at the state 3 (in the presence and absence of 2.5 µg/mL concentration of oligomycin that totally blocks ATP synthase in wild type mitochondria at pH = 6.8). The ATP synthesis rates were decreased by 25% in *Δatp19* but only by 10% in *Δmco10*. However, in the presence of oligomycin, which completely blocked ATP synthesis in *Δatp19*, its rate was twice higher in *Δmco10* in comparison to wild type mitochondria (Fig. 3c). We assessed the functioning of ATP synthase in the reverse mode by measuring the rate of ATP hydrolysis in not osmotically protected mitochondria at pH 8.4, so as to relax ATP synthase from any membrane potential that would limit its ATP hydrolytic activity, and to avoid binding to F_1 of its natural inhibitor IF1[60]. To assess the ATPase activity of ATP synthase the measurements were performed in the presence of oligomycin, which blocks efficiently rotation of *c*-ring in this condition (more efficiently than at the pH = 6.8[49]) and hence F_1-mediated ATP hydrolysis performed by coupled enzyme. In wild type mitochondria the ATPase activity is inhibited by 80–90%. The ATPase activity in the mutants was not significantly affected and efficiently inhibited by oligomycin, indicating that the enzyme is assembled and coupled (Fig. 3d). To explore deeper the increased resistance to oligomycin of ATP synthesis rate observed in *Δmco10* mitochondria and showed on panel 3c, we determined the rate of oxygen consumption and ATP production with a range of concentrations of oligomycin: 0.5, 1, 2.5 µg/mL. Oligomycin at 0.5 µg/mL inhibits the oxygen consumption by around 10–15% in wild type mitochondria (Fig. 3e). Under this suboptimal doses (0.5, 1 µg/mL), the oxygen consumption and ATP synthesis rates in *Δmco10* mitochondria were similar to the control mitochondria, but this concentration of oligomycin was sufficient to block ATP synthase in *Δatp19* and *Δatp19Δmco10* double mutant entirely (Fig. 3f).

We further investigated ATP synthase functionality in the mutant mitochondria by membrane potential (ΔΨ) measurements, using Rhodamine 123, a cationic dye whose fluorescence is quenched when ΔΨ increases. For evaluating ΔΨ changes upon respiratory chain and ATP synthase activity, the mitochondrial membrane

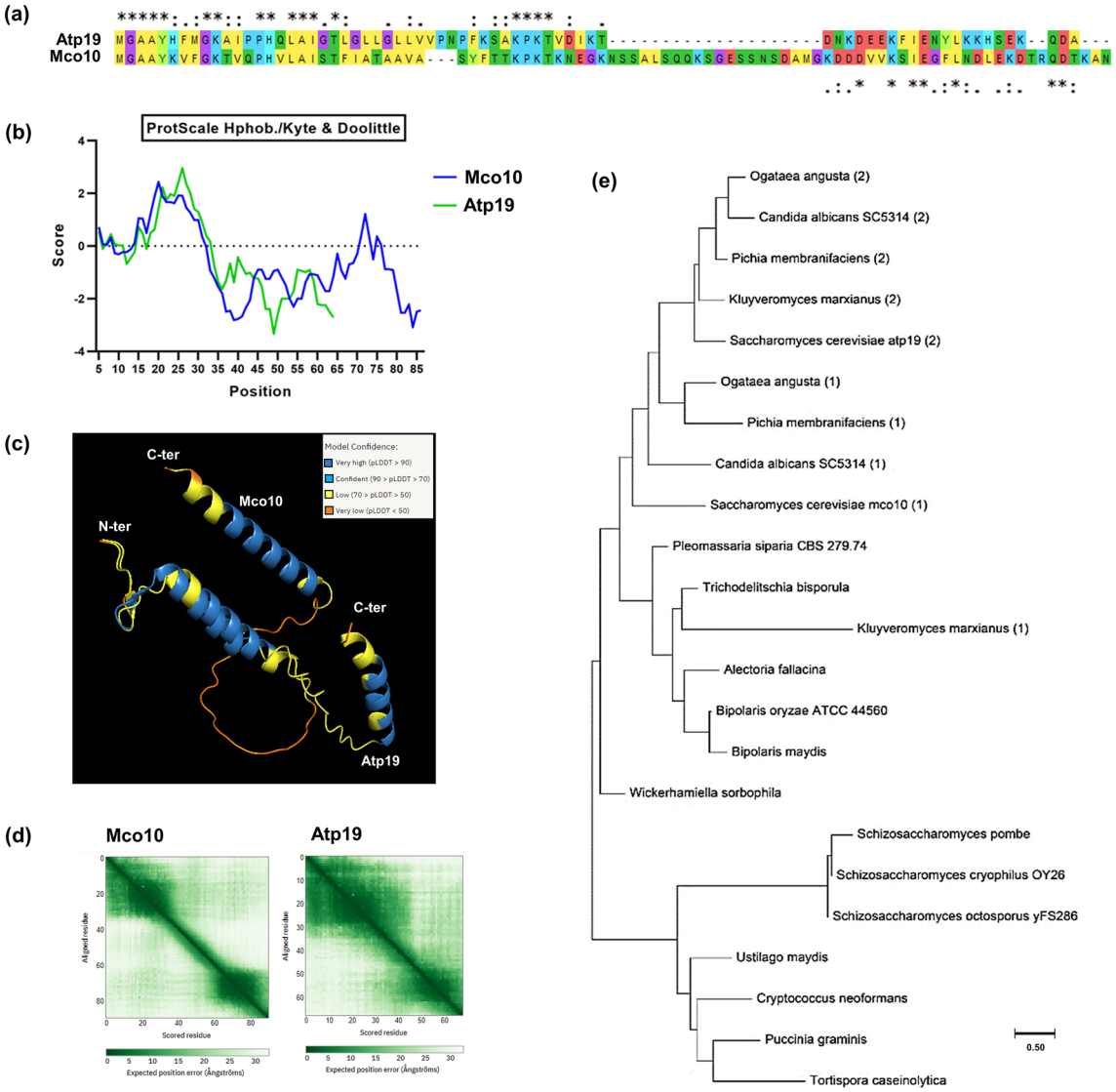

Figure 2. Mco10 and Atp19 phylogenetic and structural analysis. (**a**) Alignment of Mco10 and Atp19 sequences by Clustal Omega. (**b**) Hydropathy plots of Mco10 and Atp19 by Kate and Doolittle method using ProtScale on the ExPASy Server. (**c**) Structures of Mco10 and Atp19 as predicted in the model from AlphaFold2 database. The color code represents the model confidence as determined by the AI algorithm of AlphaFold2. The alignment was done using PyMol molecular visualization software. (**d**) AlphaFold's expected position error PAE plot of Mco10 and Atp19. (**e**) Phylogenetic tree analysis of Mco10, Atp19 and related homologs in fungi. The tree was constructed using Maximum likelihood method with representative species from all subphylum of *Ascomycota* and representative examples of *Basidiomycota*. (1) represents Mco10 related homolog and (2) represents Atp19 related homolog when there were two distinct proteins present in the genome of the organism.

was first energized by feeding the respiratory chain with electrons from ethanol. Then ADP was added what results in a transient ΔΨ drop due to proton reentry which is reestablished within one minute. Then the ΔΨ is collapsed by addition of the complex IV inhibitor KCN but then ATP synthase consumes ATP produced during previous step of the experiment and pumps protons reestablishing partially the membrane potential (Fig. 4). The ΔΨ variations during experiment were not affected in *Δmco10* and *Δatp19* but the time of ΔΨ recovery after ADP addition in the double *Δatp19Δmco10* mutant was longer. This experiment confirms a defect of about 10% in oxygen consumption and 10–20% in ATP synthesis/hydrolysis activities observed in above experiments in mitochondria lacking both Mco10 and Atp19 subunits.

Assembly/stability of ATP synthase in *Δmco10* mutant. In order to determine the Mco10 and Atp19 impact on ATP synthase complexes we extracted them from mitochondria prepared from *Δatp19*, *Δmco10* and the double deletion *Δatp19Δmco10* mutants and separated on 3–12% Blue Native PAGE, followed by Western blotting. Then 500 µg of mitochondria were incubated in extraction buffer containing 2% of digitonin for time period varying from 20 to 60 min. With higher digitonin concentration and/or longer incubation time the stability of dimers decreases (our observation based on the experiments performed on mitochondria from W303-1B

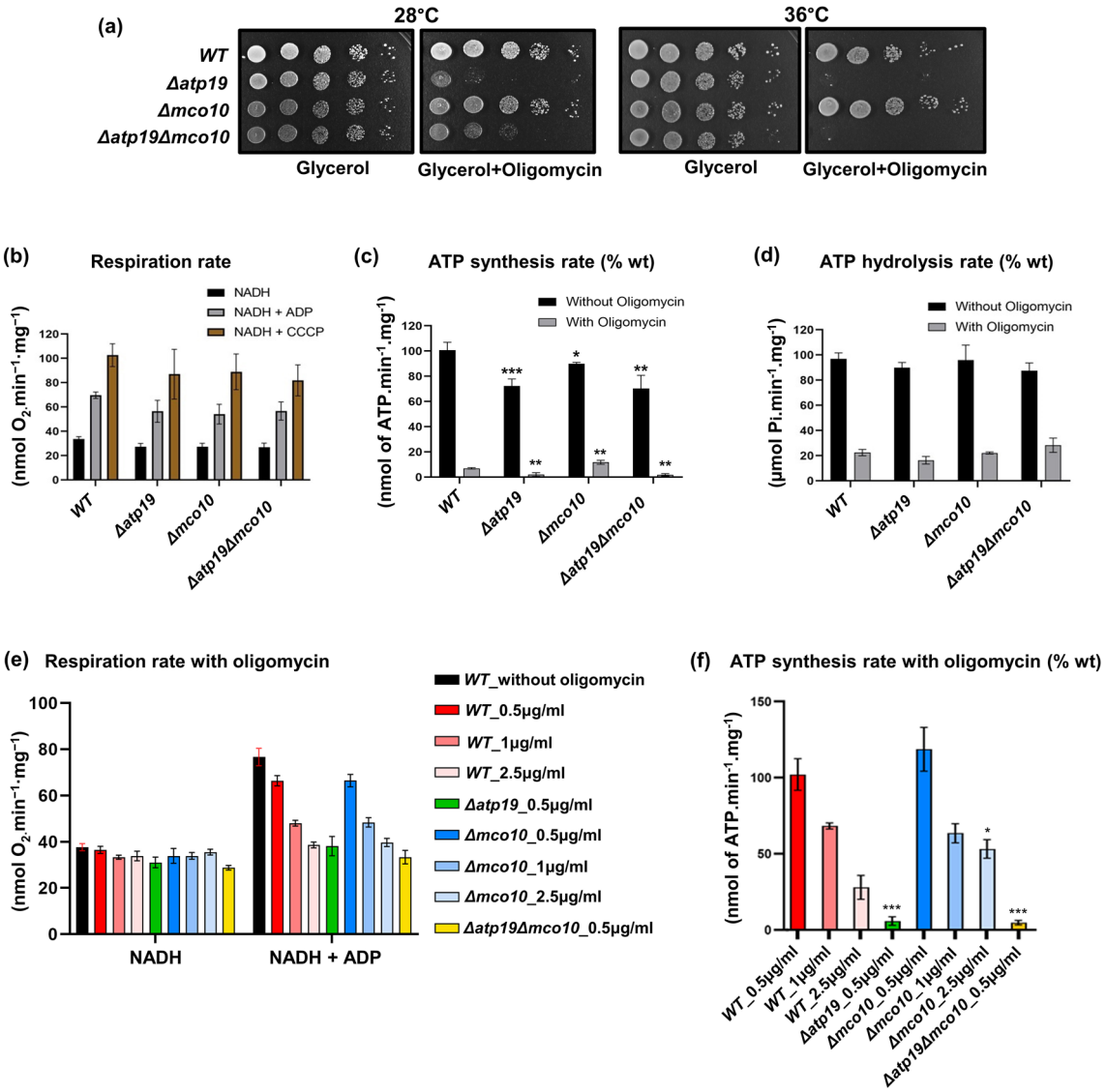

Figure 3. Respiratory growth, oxygen consumption rates and ATP synthase activities in *Δmco10*, *Δatp19* and *Δatp19Δmco10* mutants. (**a**) Respiratory growth phenotypes. Cells from the indicated strains grown in glucose pre-cultures were serially diluted and spotted on rich glucose or glycerol plates with or without oligomycin (1 µg/mL) and incubated at 28 or 36 °C. The glycerol plates were photographed after three days while the glycerol + oligomycin plates after four days of incubation. (**b**, **c**, **d**) Oxygen consumption rates, ATP synthesis and hydrolysis activities. Measurements were performed on freshly isolated mitochondria. The state 4, state 3 and maximal oxygen consumption were measured when NADH, ADP and CCCP were added. The respiration rate is expressed in percentage of the uncoupled respiration of wild type mitochondria. ATP synthesis and hydrolysis activities on panels (**c**) and (**d**) (darker rectangles) are expressed in percentage with respect to wild type mitochondria, whereas the activities in the presence of oligomycin (at 2.5 µg/mL, lighter rectangles) are expressed as the percentage of corresponding activities without oligomycin. (**e**) The oxygen consumption rate of isolated mitochondria measured in the presence of 0.5, 1 or 2.5 µg/mL of oligomycin before addition of ADP. (**f**) ATP synthesis measured in the conditions of experiment shown in panel (**e**), represented as the percentage of the ATP production in control mitochondria. Data are presented from three repetitions, statistical significance is indicated by $^{*}p \leq 0.05$; $^{**}p \leq 0.005$; $^{***}p \leq 0.001$.

strain background routinely used in our laboratory). However, in the BY4741 wild type strain mitochondria, the ATP synthase dimeric and monomeric complexes were stable after 60 min extraction time independently on the *Δmco10*, *Δatp19* single and the double *Δatp19Δmco10* deletion (Fig. 5a). Although the BN-PAGE technique is a semi-quantitative, from the ratio of dimers to monomers we conclude that much less dimers is extracted from mitochondria lacking Atp19 but not Mco10 at each extraction time. These results confirm the Atp19 role in stabilization of the dimers, as proposed by other researchers[11]. In contrast, when Mco10 is absent the ratio of dimers to monomers is not significantly changed, but more ATP synthase complexes, i.e., both the monomers and the dimers were extracted at every time point comparing to the wild type enzyme (Fig. 5a and Supplementary Fig. S6). From this we conclude that ATP synthase complexes are extracted more easily in *Δmco10* mito-

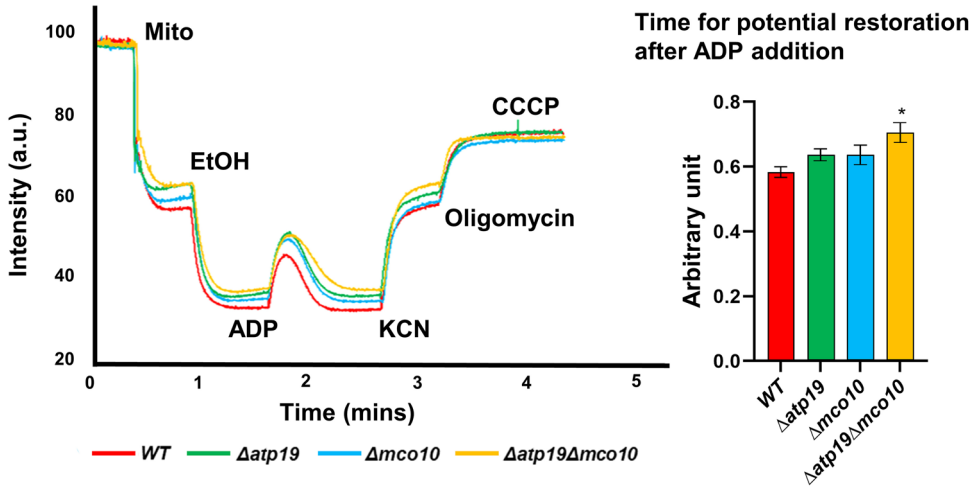

Figure 4. Variations in the mitochondrial inner membrane potential in isolated mitochondria from strains grown at 28 °C measured under osmotic protection. The additions were 0.5 µg/mL Rhodamine 123, 150 µg/mL of mitochondrial proteins (Mito), 10 µL ethanol (EtOH), 75 µM ADP, 2 mM potassium cyanide (KCN), 4 µg/mL oligomycin (oligo), and 4 µM carbonyl cyanide-m-chlorophenyl hydrazone (CCCP). Traces are representative of three independent experiments, and the histogram refers to the time that is needed for restoration of ΔΨ after ADP addition. Statistical significance of differences versus control mitochondria is indicated by $^{*}p \leq 0.05$.

chondria. Interestingly, more oligomers were also extracted from the mitochondria of the double mutant at 20 and 30 min extraction time (Fig. 5a). The steady state level of Atp7 and Atp2 subunits of ATP synthase, Cob1 and Rip1 subunits of complex III and Cox2 subunit of complex IV, analyzed in denaturing gels, was not changed in mitochondria in *Δmco10*, *Δatp19*, *Δatp20*, *Δatp21* single and the double mutants, showing no impact of Mco10 and Atp19 proteins on biogenesis of ATP synthase, as well as complexes III or IV (Fig. 5b,c).

To study the Mco10 protein levels we successfully generated a Mco10-specific antibody using the Mco10 fragment that differs from Atp19 (see Materials and Methods). Western blot analysis of the total protein extracts showed that Mco10 protein levels do not change as compared to wild type cells when Atp19 or the dimer specific subunits Atp20 and Atp21, Atp14 or Atp18 were deleted (Fig. 5b, Supplementary Fig. S7).

Mco10 mainly associates with the ATP synthase monomer. To confirm the Mco10 association with the ATP synthase we extracted its complexes, separated them in native gels and processed by Western blotting with anti-Mco10 antibody. Unfortunately, the anti-Mco10 antibody (as well as anti-Atp19 antibody used in this study) could not recognize the protein specifically in the ATP synthase monomer/dimer native complexes—probably the peptide used for immunization is not exposed in the native Mco10 or Atp19 in the whole complex (Supplementary Fig. S8a). We then applied the 2D-BN-SDS-PAGE technique as done previously with mass spectrometric analysis of the ATP synthase monomers and dimers. Western blot with anti-Mco10 antibody revealed that Mco10 is indeed present with the complex, but mainly in the monomer similarly in wild type as well as in *Δatp19*, *Δatp20 and Δatp21* mutants (Fig. 6 and Supplementary Fig. S8b). The Mco10 signal could be however detected after longer exposition time, in lane corresponding to the ATP synthase dimers. Consistently, the Atp19 is present only in the dimer of ATP synthase and its abundance is not changed when Mco10 in absent in contrast to when Atp20 is absent. Because Mco10, Atp19, Atp21 and Atp20 were detected in both the monomers and dimers in mass spectrometric analysis we applied the emPAI calculations, which gives a rough estimation of the protein's abundance. In accordance to emPAI, the Atp19 and Atp21 were respectively 16 and 100 times more abundant in the dimer when compared with the monomer while the Mco10 was 3 times more abundant in the monomer when compared with the dimer (Supplementary Fig. S8c).

Deletion of Mco10 affects calcium homeostasis and yPTP induction. Previous experiments showed that Mco10 protein is present in ATP synthase monomer and does not impact the ATP synthase activity and stability. We hypothesized then that Mco10 may be involved in the ATP synthase role in permeability transition. As transient PTP opening functions in calcium homeostasis we tested the survivability of wild type, *Δatp19*, *Δmco10*, *Δatp19Δmco10* and *Δatp21* (as a control, as lack of Atp21 delays the pore opening in yeast[19]) under high concentration of calcium in the medium. Drop test analysis showed that at 1 M Ca^{2+} in the medium, growth of *Δmco10*, *Δatp19Δmco10* and *Δatp21* were significantly more affected when compared to the wild type or *Δatp19* strain (Fig. 7a). This indicated that Mco10 deletion may affect yeast permeability transition pore (yPTP) and cell death.

To further confirm the role of Mco10 in yPTP, we analyzed the rate of yPTP opening after high calcium addition by measuring the time necessary for calcium release into the buffer using the calcium retention capacity (CRC) method. In this protocol, Ca^{2+} release occurs due to the depolarization of the membrane and therefore

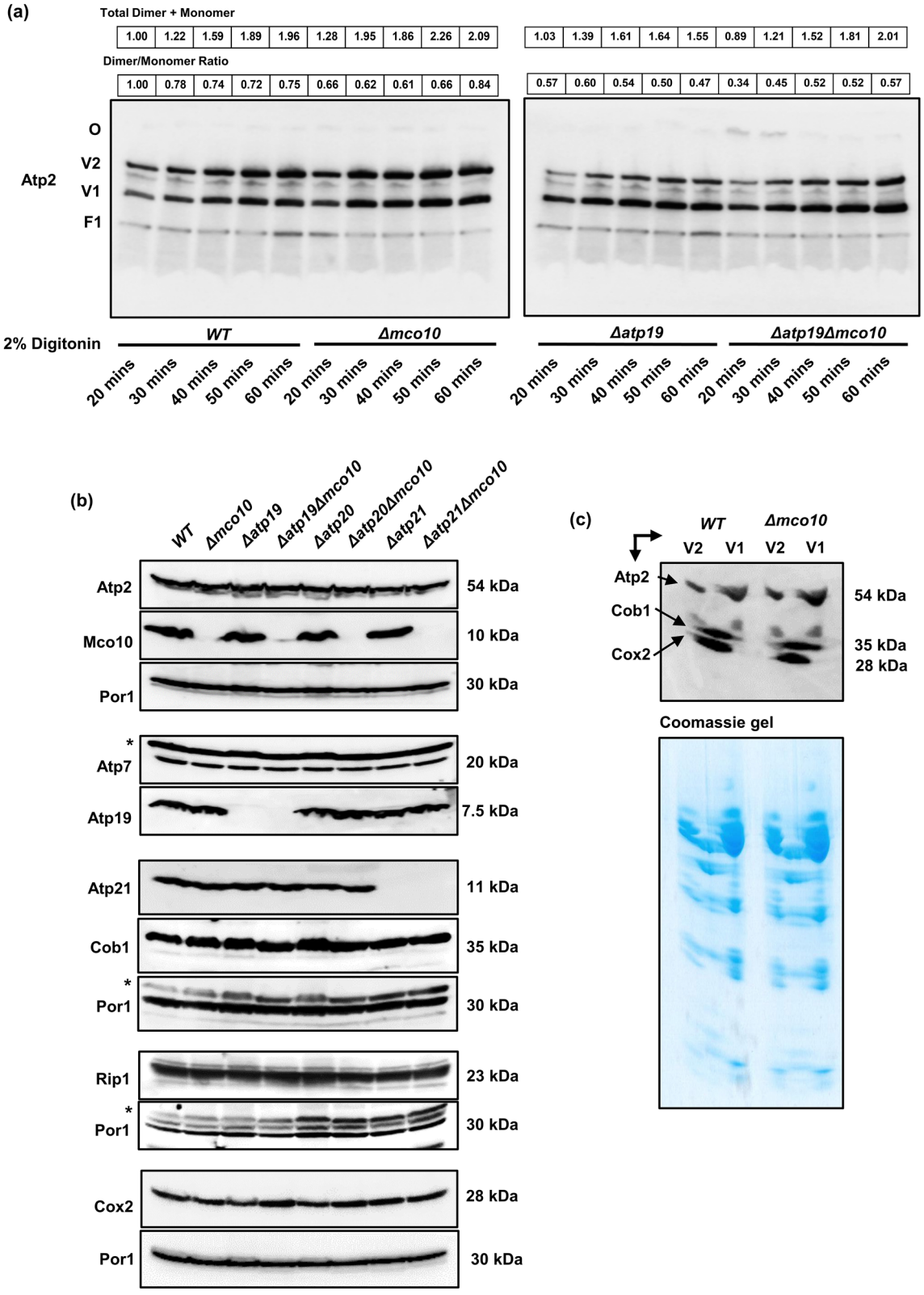

Figure 5. Mco10 deletion makes ATP synthase more susceptible to digitonin extraction. (**a**) BN-PAGE analysis of ATP synthase complexes extracted from 500 µg of mitochondria by incubation in extraction buffer containing 2% digitonin for indicated time. The dimers (V2), monomers (V1) and free F1 domain are visualized by western blot using anti-Atp2 antibody. The total amount of dimers and monomers as well as the dimers/monomers ratios are indicated above the gels. Original blots/gels are presented in SupplementaryRowImages page 2. (**b**) Western blot analysis of ATP synthase, complex III and complex IV subunits in total protein extracts from *Δmco10*, *Δatp19*, *Δatp20*, *Δatp21* and corresponding *Δmco10* double mutants grown in YPGlyA medium. Non-specific bands are indicated with the stars. Por1 protein level is shown as loading control. Original blots/gels are presented in SupplementaryRowImages pages 3–6. (**c**) Complex III, IV and ATP synthase subunits abundance in two-dimensional gel electrophoresis after digitonin extraction. The lower panel shows the Coomassie stained second dimensional denaturing gels. Original blots/gels are presented in SupplementaryRowImages page 7.The representative gels are shown.

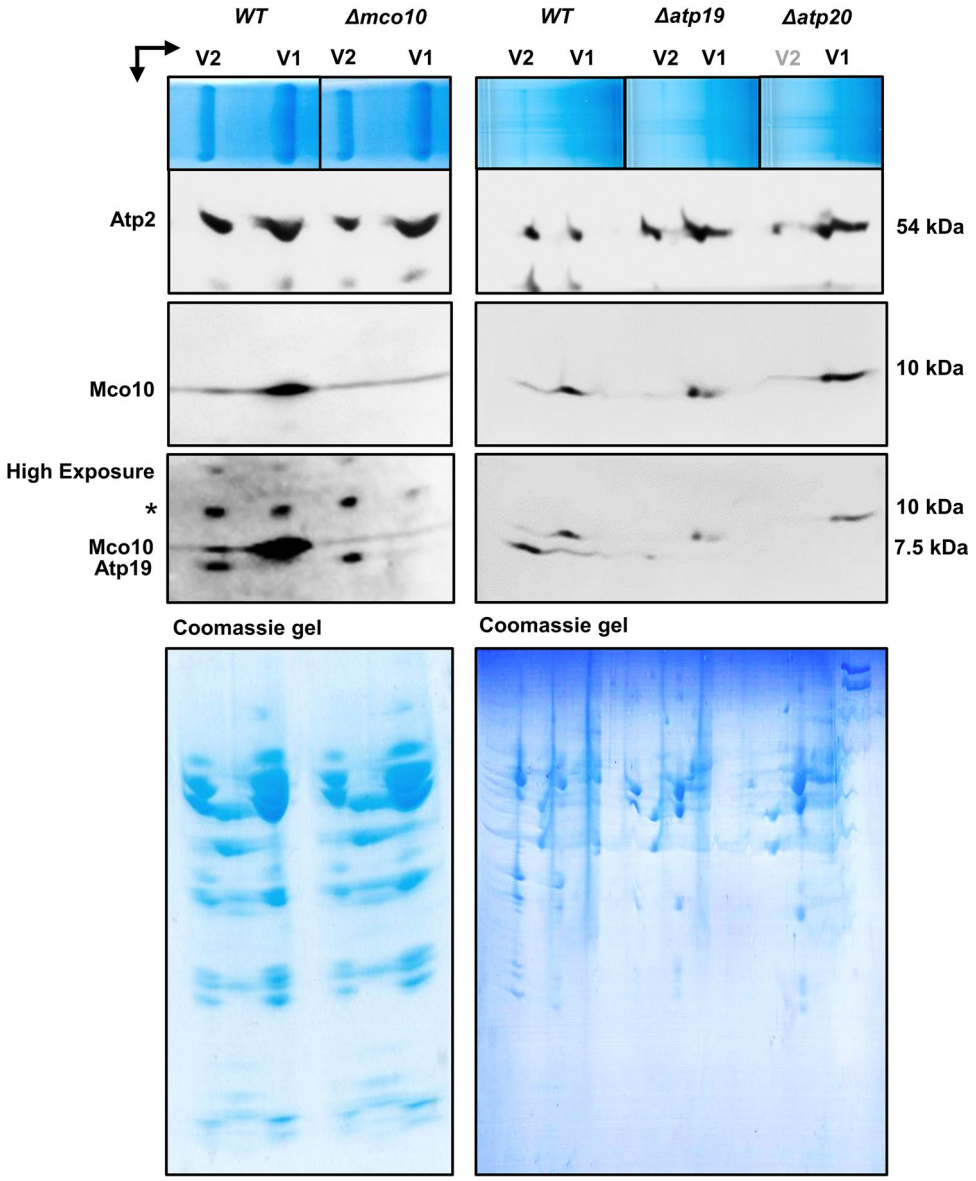

Figure 6. Mco10 is mainly present in the monomer of ATP synthase. The two-dimensional BN-SDS-PAGE gel separation of monomer and dimer subunits. After migration proteins were transferred to PVDF membrane and visualized by western blotting with respective antibodies. The upper panel shows the separation of the monomers and dimers in the first dimensional native gel. The lower panel shows the Coomassie stained second dimensional denaturing gels. Star indicates the nonspecific protein strongly recognized by anti-Atp19 antibody. Original blots/gels are presented in SupplementaryRowImages page 8. The representative gels are shown.

is compatible with the opening of a low conductance PTP[61]. Mitochondria were loaded with 200 μM $CaCl_2$, which was completely taken up into the matrix via the calcium ionophore ETH129. After 3–5 min, calcium was released into the buffer through the yPTP in the mitochondria, which was measured by the increase in florescence of Calcium Green, a cell impermeable calcium ion concentration indicator. In the wild type and *Δatp19* mitochondria the release of calcium occurred after 3 min in these experimental conditions. As expected, the absence of Atp21 decreased Ca^{2+} sensitivity of the pore which leads to increase in the time required to open the pore when compared with the wild type mitochondria[62]. Lack of Mco10 increased the yPTP opening time similarly as lack of Atp21, indicating that deletion of Mco10 significantly affects Ca^{2+} sensitivity of the yPTP. Deletion of *Δatp19* had no impact on the time of the pore opening. In the *Δatp19Δmco10* double mutant, the time needed to Ca^{2+} release was similar to that in single *Δmco10* and *Δatp21* (Fig. 7b). The experiment was also performed with pulses of 10 μM $CaCl_2$ added at an interval of 20 s until the mitochondria stops the intake of Ca^{2+} ions and finally release it into the buffer. The release of calcium was similarly slower when Mco10 was deleted under these conditions (Supplementary Fig. S9).

Next, we measured the swelling of mitochondria induced by high (2 mM) Ca^{2+} concentrations and caused by the diffusion of sucrose into the matrix. This is only possible when a large channel is formed. In this experiment,

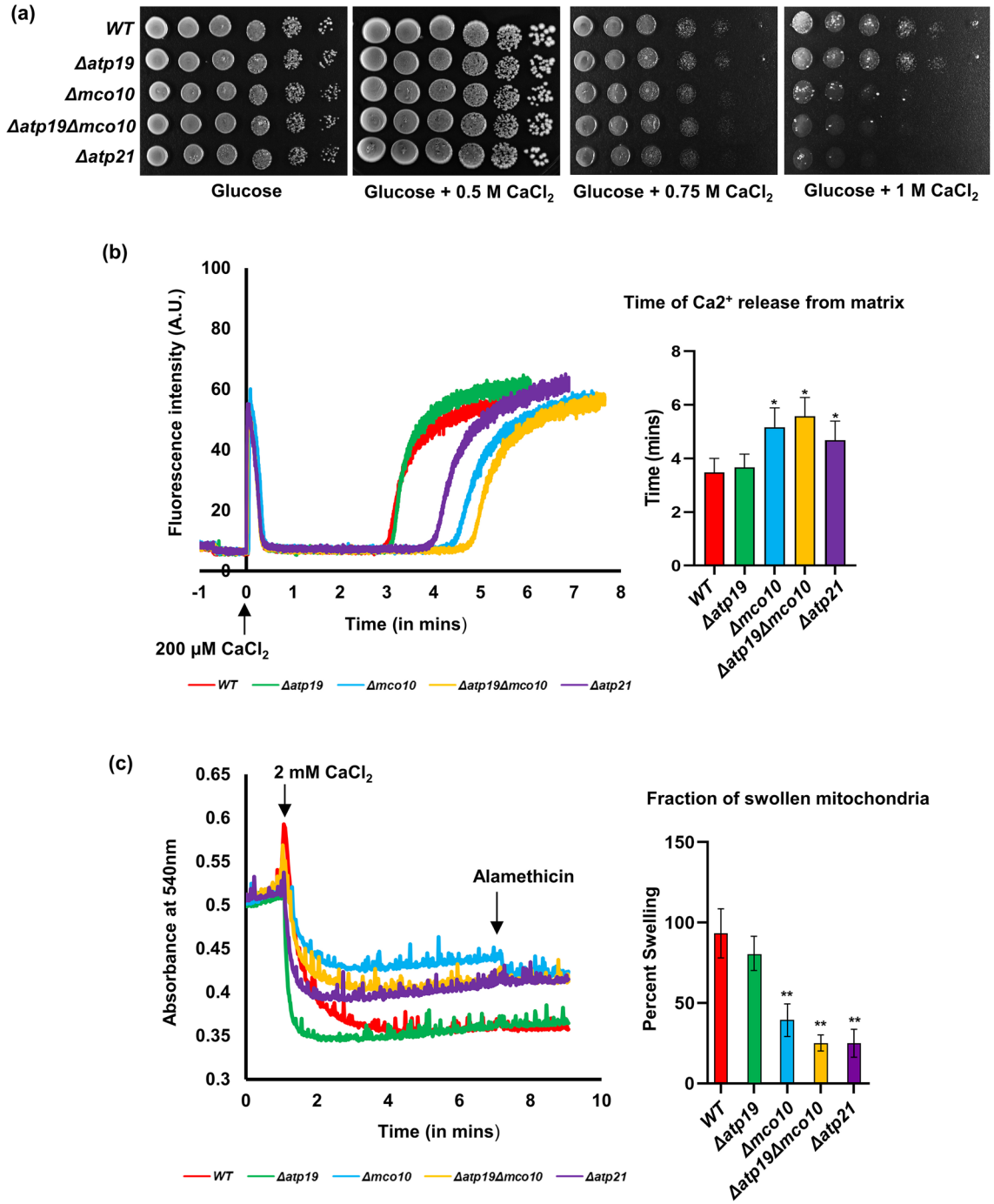

Figure 7. Mco10 modulates the yPTP. (**a**) Cells from the indicated strains grown in glucose pre-cultures were serially diluted, spotted on rich glucose plates supplemented with 0.5 M, 0.75 M and 1 M $CaCl_2$ and incubated at 28 °C. Plates were photographed after four days of incubation. (**b**) The yPTP induction time measured in the CRC experiment. 1 mg of mitochondria was added to CRC buffer containing the calcium ionophore ETH129 and the calcium green-5N calcium indicator, and 200 μM $CaCl_2$ was added at time 0. The experiment was monitored till the rapid increase of the calcium in the buffer. Traces are representative of at least 3 independent experiments and the histogram refers to the time needed for calcium release. (**c**) Mitochondrial swelling assay. Swelling was induced by the addition of 2 mM $CaCl_2$ to 1 mg of mitochondria suspended in swelling buffer containing the ETH129 and measured as the decrease in absorbance at 540 nm. Alamethicin (10 μM) was added after 2.5 min of swelling for normalization of the experiment. The histogram refers to the fraction of swollen mitochondria after completion of the process 2.5 min after calcium addition. The representative plates and curves are shown. Statistical significance of differences versus control mitochondria is indicated by $^{*}p \leq 0.05$; $^{**}p < 0.005$.

wild type mitochondria were able to form such a channel and swelled shortly after calcium addition. As expected, swelling was significantly blocked in *Δatp21* mutant mitochondria. Lack of Mco10 affected swelling similarly like lack of Atp21, while lack of Atp19 had no impact on mitochondrial swelling. Mitochondria from *Δatp19Δmco10* double mutant were also unable to swell properly (Fig. 7c). Thus, we conclude that Mco10, a new subunit of ATP synthase in *S. cerevisiae* is critical for calcium induced yPTP.

Discussion

So far three supernumerary subunits of the mitochondrial ATP synthases were identified in different experimental approaches and their presence in the enzyme dimeric structures were confirmed[9,11,63]. These three subunits: *e*/Atp21, *g*/Atp20 and *k*/Atp19, fulfil the structural role in the stabilization of the enzyme dimers[11,62,64]. An additional fungi specific subunit *l* was co-purified with the ATP synthase of *S. cerevisiae* and *P. angusta* and their homologues were fund in fungi genomes but there is no evidence that the protein is a subunit of ATP synthase, nor any indication of its biological function[36]. In our effort to purify *S. cerevisiae* ATP synthase and in-depth analysis of small proteins that interact with it, we identified Mco10 to be mainly associated with the monomer. This protein caught our attention due to its similarity to *k*/Atp19 subunit and the identification of phosphorylation at Ser-53 of Mco10 in mass spectrometry analysis. The phosphorylation of S56, S57 or S59 of Mco10 was also previously reported in a large-scale study of mitochondrial phosphoproteome[65]. These post-translational modifications were found on residues of the central hydrophilic region of Mco10. The Mco10 was not found in the crystal structures of the yeast ATP synthases what questions whether Mco10 is the subunit of ATP synthase[6,38,39,66].

Lack of Mco10 or Atp19 affected different functions of ATP synthase. In accordance to the published data, we found that Atp19 is needed for stabilization of the dimers of ATP synthase while Mco10 is not (Fig. 5a). The lack of Atp19 impacts the ATP synthesis activity of ATP synthase while lack of Mco10 has minor effect (Fig. 3c). The oligomycin sensitivity of ATP synthesis was however increased by lack of Atp19 but decreased by lack of Mco10, arguing that Mco10 is indeed attached to the enzyme and modulates oligomycin effect on the enzyme activity (Fig. 3c,e,f). The decreased ATP synthesis rate and longer time needed to recover the ΔΨ after ADP addition in the double *Δatp19Δmco10* mutant in comparison to the single mutants or wild type strain further support this conclusion. Oligomycin binds to the subunit *c* middle region of helix 2 (the external one) which is in contact with the proton half channels forming residues of subunit *a*/Atp6[67–69]. We propose that Mco10 facilitates oligomycin binding or effect on blocking of the *c*-ring rotation (see below). In *Δatp19*, more of Mco10 may be present on ATP synthase complexes therefore these complexes are more efficiently inhibited by this drug.

From the crystal structures of *S. cerevisiae* and mammalian ATP synthases, Atp19 attaches with the complex with its N-terminal helix in a V-shaped groove formed by helix 4 and 5 of subunit *a*/Atp6[6,70,71]. Basing on the conservation of the N-terminal fragments of Mco10 and Atp19 sequence and structures in *S. cerevisiae* and in other yeasts, we propose that Mco10 and Atp19 might be present in the same position in the ATP synthase F_O domain[6]. To support this hypothesis, due to lack of the full-length subunit *k*/Atp19 structures, we reconstructed the Fo domain based on the crystal structure (PDB: 6B8H) with AlphaFold2 predicted structures of each of its subunit and replaced the predicted AlphaFold2 structure of Atp19 with that of Mco10 in this model. Surprisingly, Mco10 accommodates very well in the structure with least steric hindrance with the neighboring subunit *i*/Atp18, *a*/Atp6 or the *c*-ring (Fig. 8a,b). Additionally, when Mco10 is placed at this site instead of *k*/Atp19, the packing of the Fo subunits in this region is much tighter (due to the middle loop of Mco10 which exact orientation is impossible to be predicted by AlphaFold2). This is a possible explaination why oligomycin, binding to the central region of the second helix 2 of subunit *c*[69] blocks more efficiently the rotation of the *c*-ring primed by Mco10. Although Mco10 was identified in the both monomers and dimers by mass spectrometry analysis it is more abundant in the monomer of ATP synthase in Western blot analysis. It was previously shown that *e*/Atp21, *g*/Atp20 and *k*/Atp19 subunits 'prime' the monomers before the dimers are formed[11]. Basing on the increased sensitivity to oligomycin of the ATP synthase in *Δatp19* cells and the proposition of Symersky et al.[69] that oligomycin may preferentially bind to the *c*-ring of the ATP synthases that are damaged and uncoupled (based on the previous findings that oligomycin increases phosphorylation capacity of EDTA or alkali-treated non-phosphorylating sub-mitochondrial particles[72,73]), we further propose that the ATP synthases where Mco10 binds may be uncoupled/damaged physiologically. Another very important role of Mco10, but not Atp19, for mitochondrial physiology is yPTP regulation by calcium and possibly regulation of calcium homeostasis. It is documented, also in yeast, that yPTP is delayed in the absence of the dimerization subunits *e*/Atp21 and *g*/Atp20 indicating that ATP synthase dimers are needed for channel formation[19,74,75]. Our data show that among the supernumerary ATP synthase subunits, only subunit *k*/Atp19 does not appear to be involved in formation of the mega-channel in yeast. Importantly, cells lacking Mco10 but not *k*/Atp19, similarly like those lacking *e*/Atp21 that is necessary for yPTP induction, grow slower in high concentration of calcium in the medium. Calcium homeostasis has a direct link with reactive oxygen species (ROS) generation and increase in calcium cytosolic concentration leads to cell death through mitochondrial permeability transition[76,77]. Thus, the decreased viability of Mco10 or Atp21 lacking cells in media supplemented with calcium indicates that indeed yPTP contributes to calcium buffering by its pumping into or out from the mitochondria, as we suggested previously[20]. The yeast mitochondria do not possess a known calcium transporter to the mitochondrial matrix[78–80]. The Sec61 translocation complex, subunits of which were identified in the interactome analysis of both yeast and human ATP synthase, can also contribute to this process, especially that it was shown previously to form ubiquitous Ca^{2+} leak channels in the endoplasmic reticulum[81]. Since our studies with various *atp6* mutants have shown that correlation between calcium sensitivity of growth and the swelling delay/increase is not proportional, further studies are needed to understand the involvement of PTP in calcium transport in the yeast cell[20].

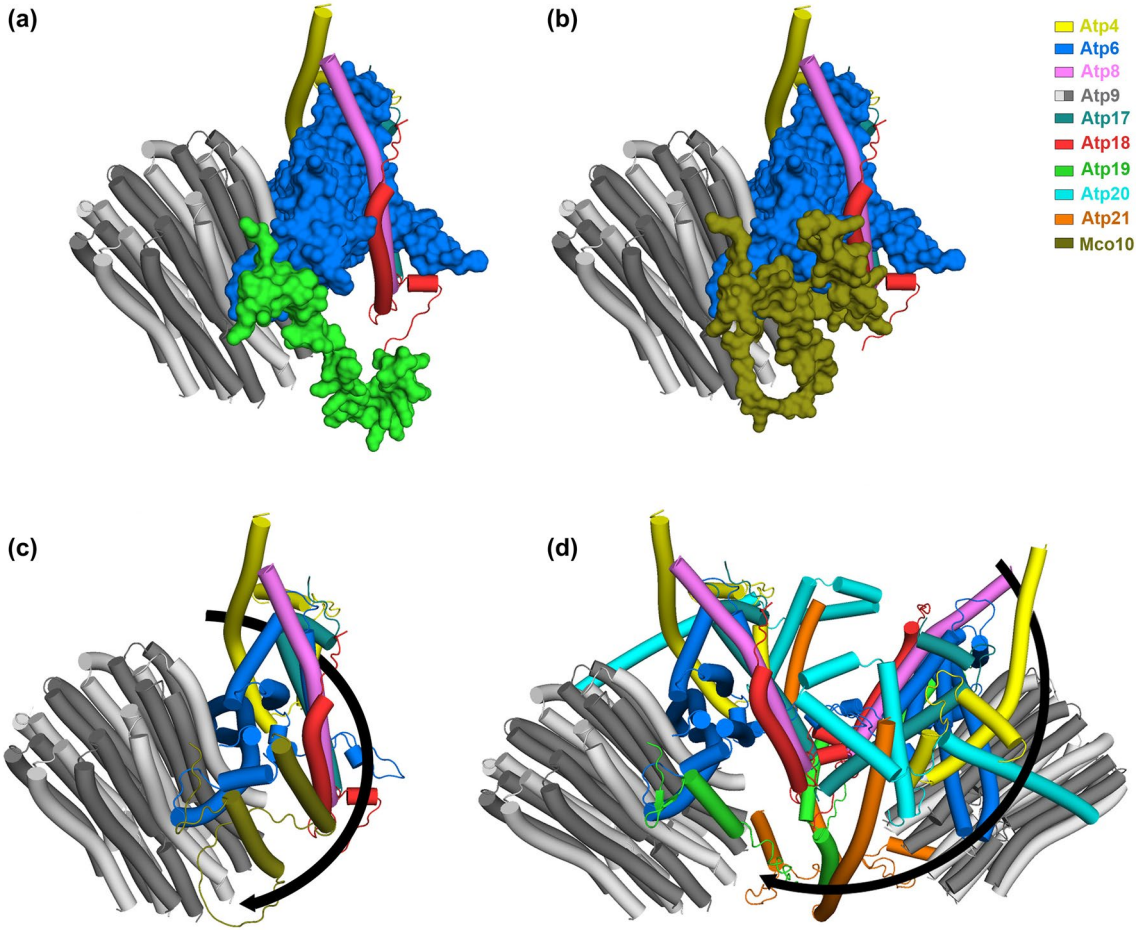

Figure 8. Remodeling of ATP synthase Fo region with AlphaFold2 predicted structures of the Fo subunits using PDB 6B8H as template and visualized in PyMOL. (**a**) Partial reconstruction of the Fo region showing *b*/Atp4 (membrane part), *k*/Atp19, *i*/Atp18, *a*/Atp6. (**b**) *k*/Atp19 is replaced by Mco10 in the model. (**c**) The PTP signal transduction pathway to the *c*-ring within the monomer of ATP synthase via b, *f*, *8*, *i*, Mco10, indicated by black arrow. (**d**) The PTP signal transduction pathway within the dimer of ATP synthase dependent on *g*/Atp20, *e*/Atp21 but not *k*/Atp21 (the b-g-e unit).

How ATP synthase forms the channel is not understood yet. One hypothesis proposes that dimerization of ATP synthase is essential for generation of the pore and pore is formed upon dissociation of the monomers[21,82] or alternatively by the F_O part of the dimer[13]. Another model proposes that ATP synthase monomer constitutes the pore forming part and its structural rearrangements within the F_O sector that perturb subunit *e*/Atp21 and may exert a pulling action dragging lipids out of the *c*-ring permitting transduction through the *c*-ring[13,17,18,83]. The ability of monomers to form PTP was also shown in mammalian liver and heart mitochondria[18,84]. The number of pores must be very limited compared with the abundance of ATP synthase in mitochondria. We propose that in yeast upon the PTP induction, in addition to the dimeric ATP synthases, the subpopulation of ATP synthase monomers 'primed' by Mco10 forms the PTP. The cryo-EM structures of ATP synthase prepared in the presence of 5 mM Ca^{2+}, when the all four obtained classes of structures had a shortened subunit *e* and disassembled *c*-ring to varying extent, indicate that the *c*-ring distortions take place during the pore opening[71]. Basing on the structural predictions shown on Fig. 8a,b, Mco10 adjusts tightly to subunits *i*/Atp18, *a*/Atp6 or the *c*-ring while *k*/Atp19 interacts only with subunit *a*/Atp6[6]. Therefore, the PTP signal induced by binding of calcium to the catalytic site of subunit β within the monomer of ATP synthase may be transmitted continuously through subunits *b*, *f*, *8*, *i*, Mco10 to the *c*-ring (Fig. 8c). Moreover, the hydrophilic middle region of Mco10 may interact with the *c*-ring what helps in maintaining an 'open' channel conformation[26]. When Mco10 is deleted, this pathway is discontinuous at the level of *i*/Atp18 and *a*/Atp6 subunits. In the dimeric ATP synthase, the PTP signal from subunit β can be transmitted to the *c*-ring of neighboring monomer by the second axis through subunits *b*, *g*/Atp20, *e*/Atp21 (the b-g-e unit), apparently without involvement of *k*/Atp19. This is more relevant in the dimer when Mco10 is largely replaced by *k*/Atp19 and the above proposed model of PTP signal transmission via *b*/*f*/*8*/*i*/Mco10 gets blocked in absence of Mco10 (Fig. 8d).

The important question that still remains unanswered is whether monomer of human ATP synthase has a functional homolog of Mco10. Although our small molecule interactome analysis did identify potential unknown modulators of yeast ATP synthase in which future research can be directed, we failed to identify such an unknown subunit/s in the human ATP synthase interactome. Based on important Mco10 role for ATP synthase function

and conservation of ATP synthase structure and function in yeast and human, it is likely that similar mechanism of PTP modulation by a specific protein that only associates with a subpopulation of ATP synthase complexes does exists in mammals. This can well be an isoform of a known ATP synthase subunit. If a functional homolog of Mco10 exists in human ATP synthase, and fulfils similar function like in yeast in modulation of PTP but not the ATP synthesis activity or dimerization of the complex, it would be an ideal target for the drugs screen for treatment of neurodegenerative diseases[26,85,86].

Data availability. The list of proteins identified in each mass spectrometry analysis from Database search using Mascot is available in Supplementary Table S1, S2 and S4.

Received: 2 November 2022; Accepted: 3 March 2023
Published online: 07 March 2023

References

1. Vakifahmetoglu-Norberg, H., Ouchida, A. T. & Norberg, E. The role of mitochondria in metabolism and cell death. *Biochem. Biophys. Res. Commun.* **482**, 426–431. https://doi.org/10.1016/j.bbrc.2016.11.088 (2017).
2. Tait, S. W. & Green, D. R. Mitochondrial regulation of cell death. *Cold Spring Harb. Perspect. Biol.* https://doi.org/10.1101/cshperspect.a008706 (2013).
3. Saraste, M. Oxidative phosphorylation at the fin de siecle. *Science* **283**, 1488–1493. https://doi.org/10.1126/science.283.5407.1488 (1999).
4. Spinelli, J. B. & Haigis, M. C. The multifaceted contributions of mitochondria to cellular metabolism. *Nat. Cell Biol.* **20**, 745–754. https://doi.org/10.1038/s41556-018-0124-1 (2018).
5. Chen, X. J. & Clark-Walker, G. D. The petite mutation in yeasts: 50 years on. *Int. Rev. Cytol.* **194**, 197–238. https://doi.org/10.1016/s0074-7696(08)62397-9 (2000).
6. Guo, H., Bueler, S. A. & Rubinstein, J. L. Atomic model for the dimeric FO region of mitochondrial ATP synthase. *Science* **358**, 936–940. https://doi.org/10.1126/science.aao4815 (2017).
7. Velours, J. *et al.* Evidence of the proximity of ATP synthase subunits 6 (a) in the inner mitochondrial membrane and in the supramolecular forms of *Saccharomyces cerevisiae* ATP synthase. *J. Biol. Chem.* **286**, 35477–35484. https://doi.org/10.1074/jbc.M111.275776 (2011).
8. Brunner, S., Everard-Gigot, V. & Stuart, R. A. Su e of the yeast F1Fo-ATP synthase forms homodimers. *J. Biol. Chem.* **277**, 48484–48489. https://doi.org/10.1074/jbc.M209382200 (2002).
9. Arnold, I., Pfeiffer, K., Neupert, W., Stuart, R. A. & Schagger, H. Yeast mitochondrial F1F0-ATP synthase exists as a dimer: Identification of three dimer-specific subunits. *EMBO J.* **17**, 7170–7178. https://doi.org/10.1093/emboj/17.24.7170 (1998).
10. Paumard, P. *et al.* The ATP synthase is involved in generating mitochondrial cristae morphology. *EMBO J.* **21**, 221–230. https://doi.org/10.1093/emboj/21.3.221 (2002).
11. Wagner, K., Perschil, I., Fichter, C. D. & van der Laan, M. Stepwise assembly of dimeric F(1)F(o)-ATP synthase in mitochondria involves the small F(o)-subunits k and i. *Mol. Biol. Cell* **21**, 1494–1504. https://doi.org/10.1091/mbc.E09-12-1023 (2010).
12. Barca, E. *et al.* USMG5 Ashkenazi Jewish founder mutation impairs mitochondrial complex V dimerization and ATP synthesis. *Hum. Mol. Genet.* **27**, 3305–3312. https://doi.org/10.1093/hmg/ddy231 (2018).
13. Bernardi, P., Carraro, M. & Lippe, G. The mitochondrial permeability transition: Recent progress and open questions. *FEBS J.* https://doi.org/10.1111/febs.16254 (2021).
14. Bernardi, P. Mechanisms for Ca(2+)-dependent permeability transition in mitochondria. *Proc. Natl. Acad. Sci. USA* **117**, 2743–2744. https://doi.org/10.1073/pnas.1921035117 (2020).
15. Haworth, R. A. & Hunter, D. R. The Ca^{2+}-induced membrane transition in mitochondria. II. Nature of the Ca^{2+} trigger site. *Arch. Biochem. Biophys.* **195**, 460–467. https://doi.org/10.1016/0003-9861(79)90372-2 (1979).
16. Azzolin, L. *et al.* The mitochondrial permeability transition from yeast to mammals. *FEBS Lett.* **584**, 2504–2509. https://doi.org/10.1016/j.febslet.2010.04.023 (2010).
17. Alavian, K. N. *et al.* An uncoupling channel within the c-subunit ring of the F1FO ATP synthase is the mitochondrial permeability transition pore. *Proc. Natl. Acad. Sci. USA* **111**, 10580–10585. https://doi.org/10.1073/pnas.1401591111 (2014).
18. Mnatsakanyan, N. *et al.* A mitochondrial megachannel resides in monomeric F1FO ATP synthase. *Nat. Commun.* **10**, 5823. https://doi.org/10.1038/s41467-019-13766-2 (2019).
19. Carraro, M. *et al.* Channel formation by yeast F-ATP synthase and the role of dimerization in the mitochondrial permeability transition. *J. Biol. Chem.* **289**, 15980–15985. https://doi.org/10.1074/jbc.C114.559633 (2014).
20. Niedzwiecka, K. *et al.* Two mutations in mitochondrial ATP6 gene of ATP synthase, related to human cancer, affect ROS, calcium homeostasis and mitochondrial permeability transition in yeast. *Biochim. Biophys. Acta Mol. Cell Res.* **117–131**, 2018. https://doi.org/10.1016/j.bbamcr.2017.10.003 (1865).
21. Giorgio, V. *et al.* Ca(2+) binding to F-ATP synthase beta subunit triggers the mitochondrial permeability transition. *EMBO Rep.* **18**, 1065–1076. https://doi.org/10.15252/embr.201643354 (2017).
22. Carraro, M. *et al.* The unique cysteine of F-ATP synthase OSCP subunit participates in modulation of the permeability transition pore. *Cell Rep.* **32**, 108095. https://doi.org/10.1016/j.celrep.2020.108095 (2020).
23. Neginskaya, M. A. *et al.* ATP synthase C-subunit-deficient mitochondria have a small cyclosporine A-sensitive channel, but lack the permeability transition pore. *Cell Rep.* **26**, 11-17 e12. https://doi.org/10.1016/j.celrep.2018.12.033 (2019).
24. Galber, C. *et al.* The f subunit of human ATP synthase is essential for normal mitochondrial morphology and permeability transition. *Cell Rep.* **35**, 109111. https://doi.org/10.1016/j.celrep.2021.109111 (2021).
25. Giorgio, V., Fogolari, F., Lippe, G. & Bernardi, P. OSCP subunit of mitochondrial ATP synthase: Role in regulation of enzyme function and of its transition to a pore. *Br. J. Pharmacol.* **176**, 4247–4257. https://doi.org/10.1111/bph.14513 (2019).
26. Mnatsakanyan, N. *et al.* Mitochondrial ATP synthase c-subunit leak channel triggers cell death upon loss of its F1 subcomplex. *Cell Death Differ.* https://doi.org/10.1038/s41418-022-00972-7 (2022).
27. Ichas, F. & Mazat, J. P. From calcium signaling to cell death: Two conformations for the mitochondrial permeability transition pore. Switching from low- to high-conductance state. *Biochim. Biophys. Acta* **1366**, 33–50. https://doi.org/10.1016/s0005-2728(98)00119-4 (1998).
28. Lemasters, J. J., Theruvath, T. P., Zhong, Z. & Nieminen, A. L. Mitochondrial calcium and the permeability transition in cell death. *Biochim. Biophys. Acta* **1787**, 1395–1401. https://doi.org/10.1016/j.bbabio.2009.06.009 (2009).
29. Bauer, T. M. & Murphy, E. Role of mitochondrial calcium and the permeability transition pore in regulating cell death. *Circ. Res.* **126**, 280–293. https://doi.org/10.1161/CIRCRESAHA.119.316306 (2020).

30. Kaludercic, N. & Giorgio, V. The dual function of reactive oxygen/nitrogen species in bioenergetics and cell death: The role of ATP synthase. *Oxid. Med. Cell Longev.* **2016**, 3869610. https://doi.org/10.1155/2016/3869610 (2016).
31. Boyenle, I. D. *et al.* Targeting the mitochondrial permeability transition pore for drug discovery: Challenges and opportunities. *Mitochondrion* **63**, 57–71. https://doi.org/10.1016/j.mito.2022.01.006 (2022).
32. Antonucci, S. *et al.* A novel class of cardioprotective small-molecule PTP inhibitors. *Pharmacol. Res.* **151**, 104548. https://doi.org/10.1016/j.phrs.2019.104548 (2020).
33. Zulian, A., Schiavone, M., Giorgio, V. & Bernardi, P. Forty years later: Mitochondria as therapeutic targets in muscle diseases. *Pharmacol. Res.* **113**, 563–573. https://doi.org/10.1016/j.phrs.2016.09.043 (2016).
34. Ebanks, B., Katyal, G., Lucassen, M., Papetti, C. & Chakrabarti, L. Proteomic analysis of the ATP synthase interactome in notothenioids highlights a pathway that inhibits ceruloplasmin production. *Am. J. Physiol. Regul. Integr. Comp. Physiol.* https://doi.org/10.1152/ajpregu.00069.2022 (2022).
35. Ahrens, C. H., Wade, J. T., Champion, M. M. & Langer, J. D. A practical guide to small protein discovery and characterization using mass spectrometry. *J. Bacteriol.* **204**, e0035321. https://doi.org/10.1128/JB.00353-21 (2022).
36. Liu, S. *et al.* The purification and characterization of ATP synthase complexes from the mitochondria of four fungal species. *Biochem. J.* **468**, 167–175. https://doi.org/10.1042/BJ20150197 (2015).
37. Morgenstern, M. *et al.* Definition of a high-confidence mitochondrial proteome at quantitative scale. *Cell Rep.* **19**, 2836–2852. https://doi.org/10.1016/j.celrep.2017.06.014 (2017).
38. Srivastava, A. P. *et al.* High-resolution cryo-EM analysis of the yeast ATP synthase in a lipid membrane. *Science* https://doi.org/10.1126/science.aas9699 (2018).
39. Vinothkumar, K. R., Montgomery, M. G., Liu, S. & Walker, J. E. Structure of the mitochondrial ATP synthase from *Pichia angusta* determined by electron cryo-microscopy. *Proc. Natl. Acad. Sci. USA* **113**, 12709–12714. https://doi.org/10.1073/pnas.1615902113 (2016).
40. He, C., Jia, C., Zhang, Y. & Xu, P. Enrichment-based proteogenomics identifies microproteins, missing proteins, and novel smORFs in *Saccharomyces cerevisiae*. *J. Proteome Res.* **17**, 2335–2344. https://doi.org/10.1021/acs.jproteome.8b00032 (2018).
41. Rak, M., Zeng, X., Briere, J. J. & Tzagoloff, A. Assembly of F0 in *Saccharomyces cerevisiae*. *Biochim. Biophys. Acta* **1793**, 108–116. https://doi.org/10.1016/j.bbamcr.2008.07.001 (2009).
42. Spelbrink, J. N. *et al.* In vivo functional analysis of the human mitochondrial DNA polymerase POLG expressed in cultured human cells. *J. Biol. Chem.* **275**, 24818–24828. https://doi.org/10.1074/jbc.M000559200 (2000).
43. Schamel, W. W. Two-dimensional blue native polyacrylamide gel electrophoresis. *Curr. Protoc. Cell Biol.* https://doi.org/10.1002/0471143030.cb0610s38 (2008).
44. Schagger, H. & von Jagow, G. Blue native electrophoresis for isolation of membrane protein complexes in enzymatically active form. *Anal. Biochem.* **199**, 223–231. https://doi.org/10.1016/0003-2697(91)90094-a (1991).
45. Kushnirov, V. V. Rapid and reliable protein extraction from yeast. *Yeast* **16**, 857–860. https://doi.org/10.1002/1097-0061(20000630)16:9%3c857::AID-YEA561%3e3.0.CO;2-B (2000).
46. Bache, N. *et al.* A novel LC system embeds analytes in pre-formed gradients for rapid, ultra-robust proteomics. *Mol. Cell Proteomics* **17**, 2284–2296. https://doi.org/10.1074/mcp.TIR118.000853 (2018).
47. Guerin, B., Labbe, P. & Somlo, M. Preparation of yeast mitochondria (*Saccharomyces cerevisiae*) with good P/O and respiratory control ratios. *Methods Enzymol.* **55**, 149–159. https://doi.org/10.1016/0076-6879(79)55021-6 (1979).
48. Rigoulet, M. & Guerin, B. Phosphate transport and ATP synthesis in yeast mitochondria: Effect of a new inhibitor: The tribenzylphosphate. *FEBS Lett.* **102**, 18–22. https://doi.org/10.1016/0014-5793(79)80919-9 (1979).
49. Somlo, M. Induction and repression of mitochondrial ATPase in yeast. *Eur. J. Biochem.* **5**, 276–284. https://doi.org/10.1111/j.1432-1033.1968.tb00368.x (1968).
50. Emaus, R. K., Grunwald, R. & Lemasters, J. J. Rhodamine 123 as a probe of transmembrane potential in isolated rat-liver mitochondria: Spectral and metabolic properties. *Biochem. Biophys. Acta.* **850**, 436–448. https://doi.org/10.1016/0005-2728(86)90112-x (1986).
51. Carraro, M. & Bernardi, P. Measurement of membrane permeability and the mitochondrial permeability transition. *Methods Cell Biol.* **155**, 369–379. https://doi.org/10.1016/bs.mcb.2019.10.004 (2020).
52. Kumar, S., Stecher, G., Li, M., Knyaz, C. & Tamura, K. MEGA X: Molecular evolutionary genetics analysis across computing platforms. *Mol. Biol. Evol.* **35**, 1547–1549. https://doi.org/10.1093/molbev/msy096 (2018).
53. Felsenstein, J. Evolutionary trees from DNA sequences: A maximum likelihood approach. *J. Mol. Evol.* **17**, 368–376. https://doi.org/10.1007/BF01734359 (1981).
54. Madeira, F. *et al.* Search and sequence analysis tools services from EMBL-EBI in 2022. *Nucleic Acids Res.* https://doi.org/10.1093/nar/gkac240 (2022).
55. Jumper, J. *et al.* Highly accurate protein structure prediction with AlphaFold. *Nature* **596**, 583–589. https://doi.org/10.1038/s41586-021-03819-2 (2021).
56. Varadi, M. *et al.* AlphaFold Protein Structure Database: Massively expanding the structural coverage of protein-sequence space with high-accuracy models. *Nucleic Acids Res.* **50**, D439–D444. https://doi.org/10.1093/nar/gkab1061 (2022).
57. Mirdita, M. *et al.* ColabFold—Making protein folding accessible to all. bioRxiv, 2021.2008.2015.456425. https://doi.org/10.1101/2021.08.15.456425 (2022).
58. Szklarczyk, D. *et al.* STRING v11: Protein–protein association networks with increased coverage, supporting functional discovery in genome-wide experimental datasets. *Nucleic Acids Res.* **47**, D607–D613. https://doi.org/10.1093/nar/gky1131 (2019).
59. Rampelt, H. *et al.* Mic10, a core subunit of the mitochondrial contact site and cristae organizing system, interacts with the dimeric F1Fo-ATP synthase. *J. Mol. Biol.* **429**, 1162–1170. https://doi.org/10.1016/j.jmb.2017.03.006 (2017).
60. Venard, R. *et al.* Investigation of the role and mechanism of IF1 and STF1 proteins, twin inhibitory peptides which interact with the yeast mitochondrial ATP synthase. *Biochemistry* **42**, 7626–7636. https://doi.org/10.1021/bi034394t (2003).
61. Niedzwiecka, K., Baranowska, E., Panja, C. & Kucharczyk, R. ATP Synthase subunit a supports permeability transition in yeast lacking dimerization subunits and modulates yPTP conductance. *Cell Physiol. Biochem.* **54**, 211–229. https://doi.org/10.33594/000000215 (2020).
62. Carraro, M. *et al.* High-conductance channel formation in yeast mitochondria is mediated by F-ATP synthase e and g subunits. *Cell Physiol. Biochem.* **50**, 1840–1855. https://doi.org/10.1159/000494864 (2018).
63. Arselin, G. *et al.* The modulation in subunits e and g amounts of yeast ATP synthase modifies mitochondrial cristae morphology. *J. Biol. Chem.* **279**, 40392–40399. https://doi.org/10.1074/jbc.M404316200 (2004).
64. Habersetzer, J. *et al.* ATP synthase oligomerization: From the enzyme models to the mitochondrial morphology. *Int. J. Biochem. Cell Biol.* **45**, 99–105. https://doi.org/10.1016/j.biocel.2012.05.017 (2013).
65. Renvoise, M. *et al.* Quantitative variations of the mitochondrial proteome and phosphoproteome during fermentative and respiratory growth in *Saccharomyces cerevisiae*. *J. Proteomics* **106**, 140–150. https://doi.org/10.1016/j.jprot.2014.04.022 (2014).
66. Hahn, A. *et al.* Structure of a complete ATP synthase dimer reveals the molecular basis of inner mitochondrial membrane morphology. *Mol. Cell* **63**, 445–456. https://doi.org/10.1016/j.molcel.2016.05.037 (2016).
67. Nagley, P., Hall, R. M. & Ooi, B. G. Amino acid substitutions in mitochondrial ATPase subunit 9 of *Saccharomyces cerevisiae* leading to oligomycin or venturicidin resistance. *FEBS Lett.* **195**, 159–163. https://doi.org/10.1016/0014-5793(86)80152-1 (1986).

68. Sebald, W., Wachter, E. & Tzagoloff, A. Identification of amino acid substitutions in the dicyclohexylcarbodiimide-binding subunit of the mitochondrial ATPase complex from oligomycin-resistant mutants of *Saccharomyces cerevisiae*. *Eur. J. Biochem.* **100**, 599–607. https://doi.org/10.1111/j.1432-1033.1979.tb04207.x (1979).
69. Symersky, J., Osowski, D., Walters, D. E. & Mueller, D. M. Oligomycin frames a common drug-binding site in the ATP synthase. *Proc. Natl. Acad. Sci. USA* **109**, 13961–13965. https://doi.org/10.1073/pnas.1207912109 (2012).
70. Spikes, T. E., Montgomery, M. G. & Walker, J. E. Interface mobility between monomers in dimeric bovine ATP synthase participates in the ultrastructure of inner mitochondrial membranes. *Proc. Natl. Acad. Sci. USA* https://doi.org/10.1073/pnas.2021012118 (2021).
71. Pinke, G., Zhou, L. & Sazanov, L. A. Cryo-EM structure of the entire mammalian F-type ATP synthase. *Nat. Struct. Mol. Biol.* **27**, 1077–1085. https://doi.org/10.1038/s41594-020-0503-8 (2020).
72. Lee, C. P. & Ernster, L. Restoration of oxidative phosphorylation in non-phosphorylating submitochondrial particles by oligomycin. *Biochem. Biophys. Res. Commun.* **18**, 523–529. https://doi.org/10.1016/0006-291x(65)90785-0 (1965).
73. Fessenden, J. M. & Racker, E. Partial resolution of the enzymes catalyzing oxidative phosphorylation. XI. Stimulation of oxidative phosphorylation by coupling factors and oligomycin; inhibition by an antibody against coupling factor 1. *J. Biol. Chem.* **241**, 2483–2489 (1966).
74. Giorgio, V. *et al.* Dimers of mitochondrial ATP synthase form the permeability transition pore. *Proc. Natl. Acad. Sci. USA* **110**, 5887–5892. https://doi.org/10.1073/pnas.1217823110 (2013).
75. Chinopoulos, C. Mitochondrial permeability transition pore: Back to the drawing board. *Neurochem. Int.* **117**, 49–54. https://doi.org/10.1016/j.neuint.2017.06.010 (2018).
76. Gorlach, A., Bertram, K., Hudecova, S. & Krizanova, O. Calcium and ROS: A mutual interplay. *Redox Biol.* **6**, 260–271. https://doi.org/10.1016/j.redox.2015.08.010 (2015).
77. Bertero, E. & Maack, C. Calcium signaling and reactive oxygen species in mitochondria. *Circ. Res.* **122**, 1460–1478. https://doi.org/10.1161/CIRCRESAHA.118.310082 (2018).
78. Carraro, M. & Bernardi, P. Calcium and reactive oxygen species in regulation of the mitochondrial permeability transition and of programmed cell death in yeast. *Cell Calcium* **60**, 102–107. https://doi.org/10.1016/j.ceca.2016.03.005 (2016).
79. Carafoli, E., Balcavage, W. X., Lehninger, A. L. & Mattoon, J. R. Ca^{2+} metabolism in yeast cells and mitochondria. *Biochim. Biophys. Acta* **205**, 18–26. https://doi.org/10.1016/0005-2728(70)90057-5 (1970).
80. Bradshaw, P. C. & Pfeiffer, D. R. Release of Ca^{2+} and Mg^{2+} from yeast mitochondria is stimulated by increased ionic strength. *BMC Biochem.* **7**, 4. https://doi.org/10.1186/1471-2091-7-4 (2006).
81. Lang, S. *et al.* Sec61 complexes form ubiquitous ER Ca^{2+} leak channels. *Channels (Austin)* **5**, 228–235. https://doi.org/10.4161/chan.5.3.15314 (2011).
82. Chinopoulos, C. ATP synthase complex and the mitochondrial permeability transition pore: Poles of attraction. *EMBO Rep.* **18**, 1041–1042. https://doi.org/10.15252/embr.201744412 (2017).
83. Bonora, M. *et al.* Role of the c subunit of the FO ATP synthase in mitochondrial permeability transition. *Cell Cycle* **12**, 674–683. https://doi.org/10.4161/cc.23599 (2013).
84. Bonora, M. *et al.* Mitochondrial permeability transition involves dissociation of F1FO ATP synthase dimers and C-ring conformation. *EMBO Rep.* **18**, 1077–1089. https://doi.org/10.15252/embr.201643602 (2017).
85. Garone, C., Pietra, A. & Nesci, S. From the structural and (Dys) function of ATP synthase to deficiency in age-related diseases. *Life (Basel)* **12**, 1. https://doi.org/10.3390/life12030401 (2022).
86. Ortiz-Gonzalez, X. R. Mitochondrial dysfunction: A common denominator in neurodevelopmental disorders?. *Dev. Neurosci.* **43**, 222–229. https://doi.org/10.1159/000517870 (2021).

Acknowledgements

We thank Prof. A. Tzagoloff for the MR6 ATP6-HisHA strain, Dr. Marie-France Giraud for the anti-ATP synthase subunits antibodies, Prof. Martin van deer Laan for anti-subunit *k* antibody, Prof. Adrianna Skoneczna for providing deletion strains from Euroscarf Library and Dr. Sampurna Datta for helping with cell culture. We also thank the IBB Mass spectrometry lab lead by Prof. Michał Dadlez and team for the help with MS analysis. This work was supported by a grant from the National Science Center of Poland (2018/31/B/NZ3/01117) to RK. The permission number for work with genetically modified microorganisms (GMM I) for RK is 01.2-28/201.

Author contributions

C.P.: Conceptualization; Data curation; Formal Analysis; Investigation; Methodology; Validation; Visualization; Writing—original draft; Writing—review and editing. A.W.: Data curation; Investigation; Writing—review and editing. K.N.: Investigation. E.B.: Investigation. R.K.: Conceptualization; Data curation; Formal Analysis; Funding acquisition; Investigation; Project administration; Resources; Supervision; Validation; Writing—original draft; Writing—review and editing. In addition to the CRediT author contributions listed above, the contributions in detail are: C.P. and R.K. project idea, C.P. designed most of the experiments, performed the work, analyzed and interpreted the data, wrote the first draft of the manuscript; A.W. performed membrane potential measurements, CRC and swelling experiments on native mitochondria and helped C.P. in conducting experiments, K.N. and E.B. performed the pull-down of ATP synthase experiments, R.K. supervised the whole work, analyzed and interpreted the data, wrote the discussion and the final text of the manuscript. All authors commented on the manuscript.

Competing interests

The authors declare no competing interests.

Additional information

Supplementary Information The online version contains supplementary material available at https://doi.org/10.1038/s41598-023-30966-5.

Correspondence and requests for materials should be addressed to C.P. or R.K.